

~~CONFIDENTIAL~~

# *Quarterly Summary Report No. 38-14*

*for the period October 1, 1963 to December 31, 1963*

(Title Unclassified)

00298

Copy No. \_\_\_\_\_

JET PROPULSION LABORATORY  
CALIFORNIA INSTITUTE OF TECHNOLOGY  
PASADENA, CALIFORNIA

January 31, 1964

~~CONFIDENTIAL~~  
~~GROUP 1~~

~~"Available to U.S. Government Agencies and  
U.S. Government Contractors Only"~~

## Preface

This report is a quarterly summary of the research activities conducted by the Jet Propulsion Laboratory in the field of nondestructive testing of solid-propellant rocket motors. Section I details the progress in specific areas of research. An introduction to the problems and objectives of the program is given in QSR 38-1; a bibliography of the subject is presented in QSR 38-1, -2, and -3; Section I of QSR 38-4 presents a general description of the subject areas covered by the entire program.

The work reported herein is undertaken in partial fulfillment of the Advanced Research Projects Agency Letter Order No. 107-60, for the National Aeronautics and Space Administration.



W. H. Pickering, Director  
Jet Propulsion Laboratory

## Quarterly Summary Report No. 38-14

Copyright © 1964, Jet Propulsion Laboratory, California Institute of Technology

Prepared under Contract No. NAS 7-100, National Aeronautics & Space Administration

This document contains information affecting the national defense of the United States, within the meaning of the Espionage Laws, Title 18, U.S.C., Sections 793 and 794, the transmission or revelation of which in any manner to an unauthorized person is prohibited by law.

## Contents

I. Physical Properties Studies . . . . .	1
A. Polymer Degradation Mechanisms: C <sup>14</sup> -Labeled Polyoxypropylene Glycol-Toluene Diisocyanate, <i>N. S. Rapp and J. D. Ingham</i> . . . . .	1
B. Application of Surfactants to Solid Propellants, <i>B. G. Moser,</i> <i>R. F. Landel, and A. J. Bauman</i> . . . . .	5
C. Ultimate Properties of Crosslinked Amorphous Gum Elastomers, <i>R. F. Fedors and R. F. Landel</i> . . . . .	11
D. Continuous Media Theory Applied to Viscoelastic Strain Analyses, V, <i>A. San Miguel</i> . . . . .	17
References . . . . .	37

## I. Physical Properties Studies

### A. Polymer Degradation Mechanisms:

#### C<sup>14</sup>-Labeled Polyoxypropylene Glycol-Toluene Diisocyanate

*J. D. Ingham and N. S. Rapp*

##### 1. Introduction

Previous work has indicated that when polyoxypropylene glycol-toluene diisocyanate (PPG-TDI) labeled at the urethane linkages with C<sup>14</sup> is heated at 200°C, the main volatile products of degradation are CO<sub>2</sub> and TDI (Ref. 1). Since diffusion of TDI at lower temperatures would be slow, especially for thick polymer or propellant samples, carbon dioxide evolution at temperatures of 75 to 200°C is being studied. The primary objectives are to establish the relationship between CO<sub>2</sub> evolution and bond scission and to learn more about the mechanism of degradation under conditions that do not favor the immediate volatilization of diisocyanate from the system. If  $n$  moles of a reactant are labeled with C<sup>14</sup> having  $A$  disintegrations per minute (dpm) in an atomic position involved in the reaction, a small amount of the product,  $\Delta n$

moles, is formed in the time  $\Delta t$  with a small amount of radioactivity,  $\Delta A$  dpm. Neglecting isotope effects,

$$A/n = \Delta A/\Delta n \quad (1)$$

the rate of formation of labeled reactant from Eq. (1) is

$$\Delta n/(V \times \Delta t) = n \times \Delta A/(V \times A \times \Delta t) \quad (2)$$

where  $n/V$  is the concentration of labeled reactant in moles per liter. The half-life  $t_{1/2}$ , for formation of the product is given by

$$t_{1/2} = 0.693 \times A(\Delta t/\Delta A) \quad (3)$$

For slow reactions the concentration of reactants should remain essentially constant and  $t_{1/2}$  should be constant for any value of  $t$ . However,  $t_{1/2}$  will depend on different initial reactant concentrations unless the reaction is first order. In studies of the decarboxylation of alanine (Ref. 2) and in this work, the rate (or  $t_{1/2}$ ) is not constant, but decreases with time, although it may decrease to a constant rate after the initial rapid evolution of C<sup>14</sup>O<sub>2</sub>. It may be that reactive intermediates (possibly peroxides) are present at very small concentrations that change significantly during C<sup>14</sup>O<sub>2</sub> evolutions of the order of 0.2 wt %

of the amount initially present as urethane, and thus affect the rate of  $C^{14}O_2$  evolution.

## 2. Experimental

Toluene diisocyanate labeled at the isocyanate groups was prepared as described previously (Ref. 3). The PPG-TDI polymers were prepared from 13.54 g of PPG of molecular weight  $\sim 2000$  and 1 cc of labeled diisocyanate and cured for 16 hr at  $142^\circ C$  under nitrogen. The degradation apparatus consisted of two tubes connected by a large (10-mm) bore stopcock. One tube contained the polymer and had a helium inlet that extended below the polymer surface. Both sides of the apparatus were provided with inert gas inlets and vent stopcocks. The cold side was large enough to contain a standard 22-ml counting vial containing 1 ml of phenethylamine for  $CO_2$  trapping. The degradation tube was heated with refluxing  $CCl_4$  ( $76.5^\circ C$ ), refluxing toluene ( $110.2^\circ C$ ) or a  $150^\circ C$  oil bath. During  $CO_2$  trapping the cold side was immersed in ice water. Trapping periods of 6 hr were used at  $76.5$  and  $110.2^\circ C$ . At  $150^\circ C$  the degradation tube was open to the cold side except when taking samples or replacing phenethylamine solution. Both sides of the tube were purged with dry helium or nitrogen when taking samples, but not during degradation. Intrinsic viscosities and activities were determined as described earlier (Ref. 3).

## 3. Results and Discussion

Results obtained so far at  $76.5$ ,  $110.2$  and  $150^\circ C$  are shown in Figs. 1 and 2, in which fraction of radioactivity lost as  $C^{14}O_2$  versus time is plotted. At  $76.5^\circ C$  the rate was constant until about 400 hr, and then decreased. At sufficiently long times it may decrease to a constant rate. However, since time is a factor, the temperature of the same sample was increased to  $110.2^\circ C$ . At this temperature, the rate is again decreasing. If it does not reach a constant value within reasonable limits of patience, the temperature will be increased and then decreased, and the rates at  $76.5$  and  $110.2^\circ C$  will be redetermined, particularly to establish if they are constant. At  $150^\circ C$ , it appears that a constant rate was obtained after  $\sim 300$  hr, with an accelerated rate between 800 and 1000 hr. It is believed that this break was caused by inadvertent admission of air to the system. For comparison with rates at lower temperatures, a part of this curve is also shown in Fig. 1.

The intrinsic viscosities for the polymers and  $C^{14}O_2$  evolution are shown in Tables 1, 2 and 3. The data in Table 3 were reported previously and discussed in terms

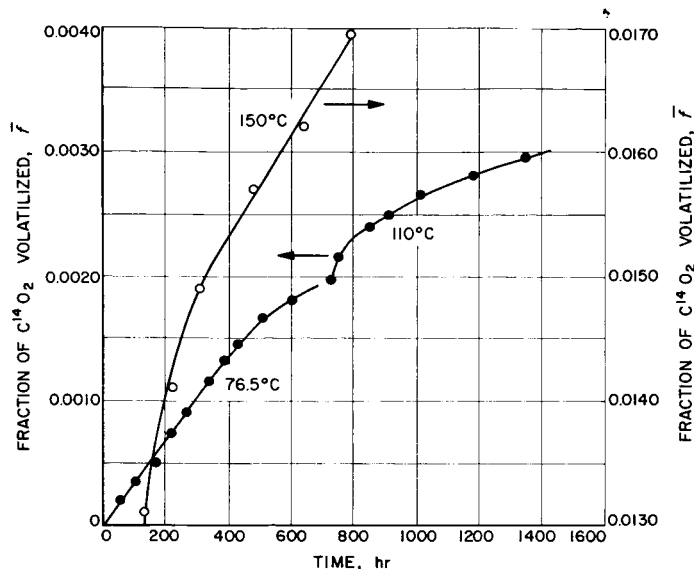


Fig. 1. Fraction of  $C^{14}O_2$  volatilized at various temperatures during degradation of PPG-TDI

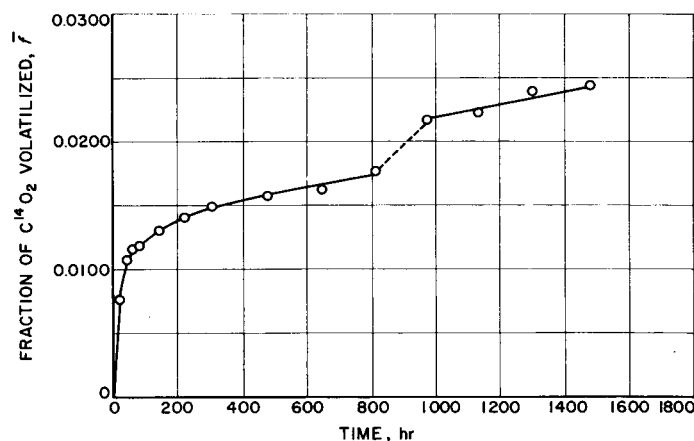


Fig. 2. Fraction of  $C^{14}O_2$  volatilized at  $150^\circ C$  from PPG-TDI

of TDI and  $C^{14}O_2$  evolution (Ref. 1), but are included here for comparison with data at the lower temperatures. In Table 1 it can be seen that at  $76.5^\circ C$  the intrinsic viscosity increases. The difference between 1.36 and 1.31 dl/g (after 600 and 725 hr) may not be significant because the polymer was very viscous and therefore not well stirred during helium purging; as a result viscosity errors could arise because of inhomogeneity of the samples. It is believed that this represents the highest molecular weight PPG-TDI polymer ever prepared and provides a method for preparing high molecular weight polyurethanes in the absence of catalyst when time is not important. At  $110.2^\circ C$  scission took place with an initially increased rate of evolution of  $C^{14}O_2$  that had been decreasing (Table 1 and

Table 1. Change in intrinsic viscosity and carbon-14 activity of PPG-TDI at 76.5 and 110.2°C

Temperature, °C	Time, hr	Intrinsic viscosity $[\eta]$ , dl/g	Wt avg mol wt, $M_w^a$	No. avg mol wt, $M_n^b$	No. of unlinked bonds, $S^c$	Fraction of unlinked bonds, $\alpha^d$	Fraction of $C^{14}$ lost as $C^{14}O_2$ , $f_0$	Fraction of $C^{14}$ lost as $C^{14}O_2$ during scission <sup>e</sup> , $f$
76.5	0	0.412	49,000	25,500	5.216	0.0666	0	
	100	0.627	95,000	48,500	2.268	0.0290	0.000352	
	220	0.754	126,000	64,000	1.477	0.0189	0.000732	
	436	1.052	210,000	106,000	0.495	0.00633	0.00146	
	508	1.048	210,000	106,000	0.495	0.00633	0.00167	
	604	1.362	315,000	158,500	0	0	0.001795	0
	725	1.305	297,000	149,500	0.060	0.000767	0.001975	0.000180
110.2	748	0.918	172,000	87,000	0.822	0.0105	0.002160	0.000365
	846	0.940	180,000	91,000	0.742	0.00948	0.002389	0.000594
	916	1.039	208,000	105,000	0.510	0.00652	0.002482	0.000687
	1014	0.903	170,000	86,000	0.843	0.0108	0.002648	0.000853
	1181	0.913	172,000	87,000	0.822	0.0105	0.002815	0.00102
	1349	0.878	162,000	82,000	0.933	0.0119	0.002947	0.00115

<sup>a</sup>Calculated from  $[\eta] = 0.413 \times 10^{-4} M_w^{0.64}$ <sup>b</sup>From  $M_n = (M_w + M_u)/2$ , assuming  $M_u = 2000$ .<sup>c</sup>From  $S = [X_{n(t)}/X_{n(0)}] - 1$ ;  $X_n = M_n/2000$ .<sup>d</sup>From  $\alpha = S/(X_{n(0)} - 1)$ .  $S$  and  $\alpha$  are ordinarily calculated after scission occurs; here values are shown before polymerization to the maximum chain length,  $X_{n(0)}$ .<sup>e</sup>The fraction of  $C^{14}O_2$  evolved before scission is subtracted to obtain these values.

Table 2. Change in intrinsic viscosity and carbon-14 activity of PPG-TDI at 150°C

Time, hr	Intrinsic viscosity $[\eta]$ , dl/g	Wt avg mol wt, $M_w^a$	No. avg mol wt, $M_n^b$	No. of unlinked bonds, $S^c$	Fraction of bonds unlinked, $\alpha^d$	Fraction of $C^{14}$ lost as $C^{14}O_2$ , $f_0$	Fraction of $C^{14}$ lost as $C^{14}O_2$ during scission <sup>e</sup> , $f$
0	0.320	33,000	17,500	0.257	0.0257	0	
20	0.338	36,000	19,000	0.158	0.0158	0.0077	
40	0.345	37,000	19,500	0.128	0.0128	0.0107	
60	0.348	37,500	19,750	0.114	0.0114	0.0116	
80	0.373	42,000	22,000	0	0	0.0119	0
150	0.336	36,000	19,000	0.158	0.0158	0.0131	0.0012
220	0.329	34,500	18,250	0.205	0.0205	0.0141	0.0022
478	0.322	33,500	17,750	0.239	0.0239	0.0157	0.0038
645	0.319	32,500	17,250	0.275	0.0275	0.0162	0.0043
811	0.318	32,300	17,150	0.283	0.0283	0.0178	0.0059
977	0.305	30,500	16,250	0.354	0.0354	0.0217	0.0098
1144	0.290	28,200	15,100	0.457	0.0457	0.0223	0.0104
1310	0.285	27,500	14,750	0.492	0.0492	0.0240	0.0121
1478	0.287	27,700	14,850	0.481	0.0481	0.0244	0.0125

<sup>a</sup>Calculated from  $[\eta] = 0.413 \times 10^{-4} M_w^{0.64}$ <sup>b</sup>From  $M_n = (M_w + M_u)/2$ , assuming  $M_u = 2000$ .<sup>c</sup>From  $S = [X_{n(t)}/X_{n(0)}] - 1$ ;  $X_n = M_n/2000$ .<sup>d</sup>From  $\alpha = S/(X_{n(0)} - 1)$ .  $S$  and  $\alpha$  are ordinarily calculated after scission occurs; here values are shown before polymerization to the maximum chain length,  $X_{n(0)}$ .<sup>e</sup>The fraction of  $C^{14}O_2$  evolved before scission is subtracted to obtain these values.

Table 3. Change in intrinsic viscosity and carbon-14 activity of PPG-TDI at 200°C

Sample No.	Time, hr	Intrinsic viscosity $[\eta]$ , dl/g	Wt avg mol wt, $M_w^a$	No. avg mol wt, $M_n^b$	No. of cuts, $S^c$	Fraction of bonds cut, $\alpha^d$	Fraction of $C^{14}$ activity lost as $C^{14}O_2$ , $\alpha/\bar{f}$	Initial NCO/OH ratio
1	0	0.339	46,500	24,250	0	0	0	1.05
	16.0	0.262	24,200	13,100	0.851	0.0765	0.020	
2	0	0.306	31,000	16,500	0	0	0	
	66.5	0.197	15,500	8,750	0.886	0.122	0.062	1.05
3	0	0.380	41,700	21,850	0	0	0	
	113.0	0.172	12,500	7,250	2.318	0.234	0.098	1.05
4	0	0.319	32,500	17,250	0	0	0	0.963
	113.0	0.176	12,800	7,400	1.331	0.175	0.057	
5 <sup>e</sup>	0	0.379	43,000	22,500	0	0	0	
	114.0	0.211	17,050	9,525	1.362	0.133	0.056	0.963

<sup>a</sup>Calculated from  $[\eta] = 0.413 \times 10^{-4} M_w^{0.64}$

<sup>b</sup>From  $M_n = (M_w + M_u)/2$ , assuming  $M_n = 2000$ .

<sup>c</sup>From  $S = [X_{n(0)}/X_{n(t)}] - 1$ ;  $X_n = M_n/2000$ .

<sup>d</sup>From  $\alpha = S/(X_{n(0)} - 1)$ .

<sup>e</sup>This polymer was degraded in dry nitrogen but not purged continuously; Nos. 1-4 were purged with dry nitrogen continuously at a flow rate of 200 ml/min during degradation.

Fig. 1). These results indicate that for PPG-TDI at room temperature scission would not be expected and that a sort of ceiling temperature exists between 75 and 110°C.

Extrapolation of high temperature data to ambient conditions for these polymers could obviously lead to unreasonable conclusions. At 150°C there was also an initial increase in molecular weight; however, it is likely that scission was occurring simultaneously, since the maximum intrinsic viscosity obtained was only 0.37 dl/g (Table 2). By comparison with Figs. 1 and 2 it can be seen that shortly after scission became dominant, the rate of  $C^{14}O_2$  evolution was constant except for the break in the curve discussed previously. Table 3 shows the results at 200°C. Since the shortest time for which measurements were made was 16 hr, the molecular weight may have first increased, although it is likely that scission was dominant early during the heating period. These results are not strictly comparable with the data at lower temperatures, because only No. 5 was run without a continuous nitrogen purge and the NCO/OH ratio for preparing Nos. 1, 2 and 3 was 1.05, and, for 4 and 5, 0.963. Estimates of the fraction of urethane bonds cut,  $\alpha$ , and the fraction

of  $C^{14}O_2$  volatilized after scission starts are given in Tables 1, 2 and 3 and in Fig. 3. There is considerable scatter in the data, especially at 200°C, for the reasons mentioned above; also at this temperature each point represents a polymer of different initial molecular weight. However, some interesting features of the results can be pointed out. The results for 110°C (dark points) are plotted on a twentyfold expanded scale. For this temperature and this low extent of degradation the ratio of fraction of urethane bonds cut to fraction of  $C^{14}O_2$  evolved,  $\alpha/\bar{f}$ , is  $\sim 10$ . For the data at 150°C,  $\alpha/\bar{f}$  is  $\sim 3$  and at 200°C may be further reduced to 2 or less. This indicates that at low values of  $\alpha$ , under conditions unfavorable for scission by the volatilization of TDI, most of the cuts occur by some other reaction than volatilization of  $C^{14}O_2$ . Again it appears that some other scission reaction takes place, possibly peroxide or other weak bond rupture. Considering the results at 200°C,  $\alpha/\bar{f}$  for No. 5 is less than for No. 4, which is expected, since the latter was purged with nitrogen continuously, thus allowing scission by TDI volatilization leaving fewer urethane bonds that can be broken to evolve  $C^{14}O_2$ . For Nos. 1, 2 and 3,  $\alpha/\bar{f}$  should be less than for 4 and 5, since the NCO/OH ratio was less

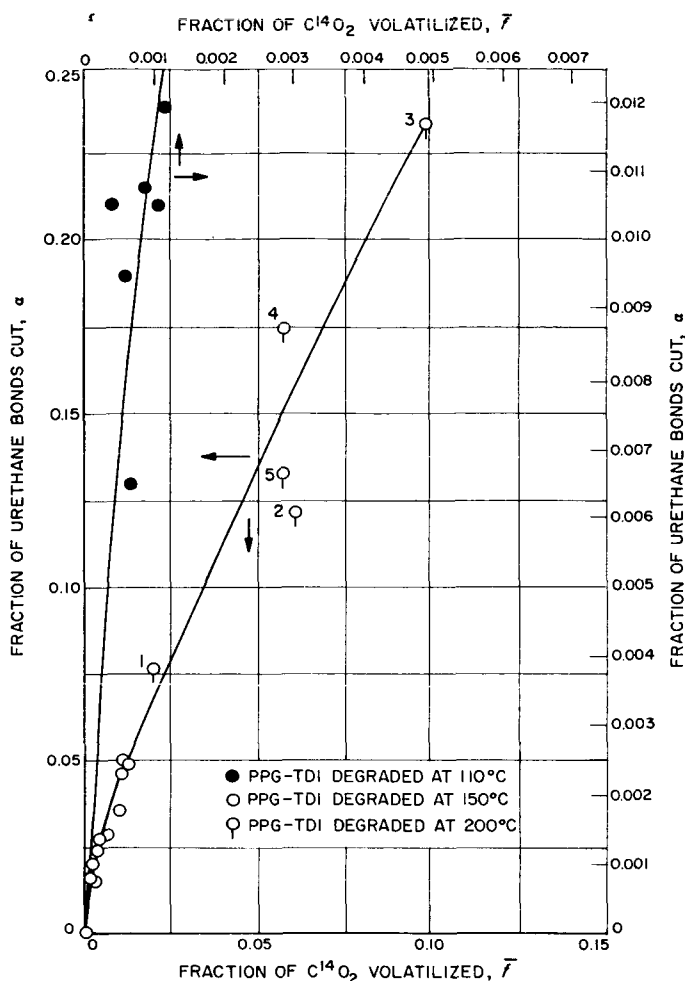


Fig. 3. Fraction of urethane bonds cut vs fraction of  $C^{14}O_2$  volatilized

for 4 and 5; that is, the higher the initial excess of isocyanate the larger the expected evolution of  $C^{14}O_2$  per scission. It appears then that the large scatter for the data at 200°C can be qualitatively explained on the basis of changes in known experimental variables.

#### 4. Conclusion

The use of radioactive tracers for degradation studies can provide useful information about the mechanism of slow degradation reactions at specific bond sites at moderate temperatures. Thus far, an approximate "ceiling" temperature for scission has been determined for PPG-TDI; a weak bond scission reaction that may not involve urethane bonds has been indicated, and an approximate empirical relationship between scission and  $C^{14}O_2$  evolution has been established for low extents of degradation.

## B. Application of Surfactants to Solid Propellants

B. G. Moser, A. J. Bauman, and R. F. Landel

### 1. Introduction

Previous reports (QSR 38-11, 38-12, 38-13, SPS 37-20, Vol. IV, Refs. 4, 5) have shown that there is an optimum concentration of a given surfactant in a given slurry system to produce a minimum viscosity. In earlier work it was not generally recognized that such an optimum existed, that the surfactant concentration at that optimum was very low (on the order of 0.2 wt %), and that the reactivity of many surfactants with the binder made adjustment of reagent parameters necessary.

The use of surfactants in solid propellants to reduce the mix viscosity has two important implications: first, the possibility of higher  $I_{sp}$ ; secondly, the capability of mixing higher solids loaded propellant makes it possible to include a small percentage of prilled or porous oxidizer without reducing the propellant density. It is postulated that the prilled oxidizer, by introducing a vastly increased burning surface, will increase the burning rate proportionally.

A third advantage that may be realized ultimately from the use of surfactants is an increased bond between the filler and the binder. If the polar group of a surfactant can be made to chemically react with, or to sorb strongly onto, the filler surface, and the nonpolar hydrocarbon tail can be made to react with the binder during the cure, then there is the possibility of improved physical properties as well. Unfortunately the mechanism of adsorption, not to mention the viscosity-reducing properties, of surfactants onto solid salt surfaces from nonaqueous media is poorly understood. A series of experiments, designed to measure and explain these unknown factors, is currently under way and will be reported later. If the experiments are successful, "tailor made" surface active agents can probably be made to fit specific requirements.

In the meantime work has been done using asolectin, a phospholipid mixture derived from soybeans. In the references listed above, the effect of this surfactant on the viscosity of ammonium perchlorate, copper powder, aluminum powder, and glass beads slurried in POPG and mineral oil was reported. In addition, an equation and "master curve" that fitted all the available data was presented in Ref. 4.

This current paper reports the effects of asolectin on the viscosity of 100  $\mu$  HMX and RDX (hexanitrodiphenylamine and trinitrotrimethylenetriamine, respectively) in the same media; it reports the fit of this viscosity data to the master curve; and it reports the effect of the surfactant on the physical properties and burning rate of a model ammonium perchlorate-polyurethane propellant.

## 2. Experimental

**a. HMX and RDX viscosity.** The HMX and RDX were mixed in a 50-g sigma blade mixer at the Naval Ordnance Test Station (NOTS), China Lake, California. A maximum of 0.2% (based on the filler) of surfactant was added to the homogeneous mixes in a solution of approximately 2 ml of anhydrous ether; the ether was removed by an additional 20 min of mixing under a vacuum. The viscosity of the slurries was determined with a parallel plate viscometer and a 16-mm movie camera as described in Ref. 4. The parallel plate viscometer was used instead of the simpler and faster glass plate method (also described in Ref. 4 and in previous QSR's) because the hazard of working with HMX and RDX made manual addition of surfactants quite inadvisable.

The maximum volume percent solids possible in the two-liquid media used (POPG MW 2020, and USP mineral oil) was measured by a centrifuge technique, also described in Ref. 4. Unfortunately the centrifuge available at NOTS was too slow for the purpose and the  $\phi_m$  measurements are inconclusive. Until the experiment can be repeated here at JPL, an approximate value is assumed. This value (although admittedly a guess), based on our considerable experience in making these measurements, is quite reasonable, and is probably not wrong by more than 2%.

**b. Burning rate.** Two model propellants, 64 wt % ammonium perchlorate, 16 wt % aluminum powder and 20 wt % polyurethane binder (POPG 2020); and 71 wt % ammonium perchlorate, 16 wt % aluminum and 13% polyurethane were formulated to study the effects of surfactant on the tensile properties and burning rate of highly loaded systems. The mixing was done on a small scale, using a 1000-g sigma blade mixer, cast under a vacuum and cured. The isocyanate to hydroxyl ratio, the percent cross linker, and the cure time were varied to find the optimum formulation, both with and without surfactant.

In all mixes 0.2-wt. % asolectin was the surfactant used. Effectiveness curves run previously (QSR 38-11) indicated that this was approximately the optimum sur-

factant concentration for 80-wt % solids AP polyurethane systems. On the other hand, preliminary effectiveness curves on an 87-wt % loaded slurry containing 2% aluminum would indicate maximum fluidity at about 0.09 wt %. Nevertheless, the 87 wt % batch which was used to measure the burning rate contained 0.2 wt % surfactant. Of course, further study on a 16% aluminum system may definitely indicate a need to reduce this figure. Again, as with the HMX and RDX mixes, the surfactant was added in an anhydrous ether solution and the ether was removed by further mixing under a vacuum.

Tensile data was obtained from milled JANAF bars,  $0.5 \times 0.375$  in. with an assumed gauge length of 2.7 in. The bars were pulled on the Instron at 2.0 in./min and 80°F. Burning rates on the 87 wt % system were measured in a bomb over a pressure range from 250 to 2000 psi. The resulting curve was compared with extensive burning rate data from JPL X-547 (Syncom) propellant, a 64% AP and 16% Al polyurethane propellant. Although experiments are under way, no burning rate data employing prilled oxidizer is yet available.

## 3. Results

**a. Effectiveness curves of HMX and RDX.** Figs. 4 through 6 are log-log plots of fluidity  $1/\eta$  versus the weight percent surfactant (based on the filler). Unfortunately time and facilities available to us at NOTS did not

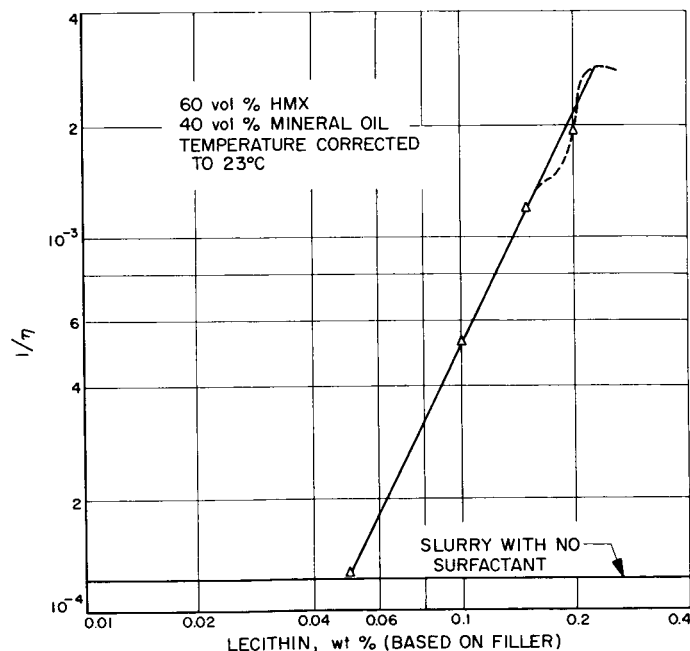


Fig. 4. Effectiveness curve  $1/\eta$  of asolectin on HMX in mineral oil

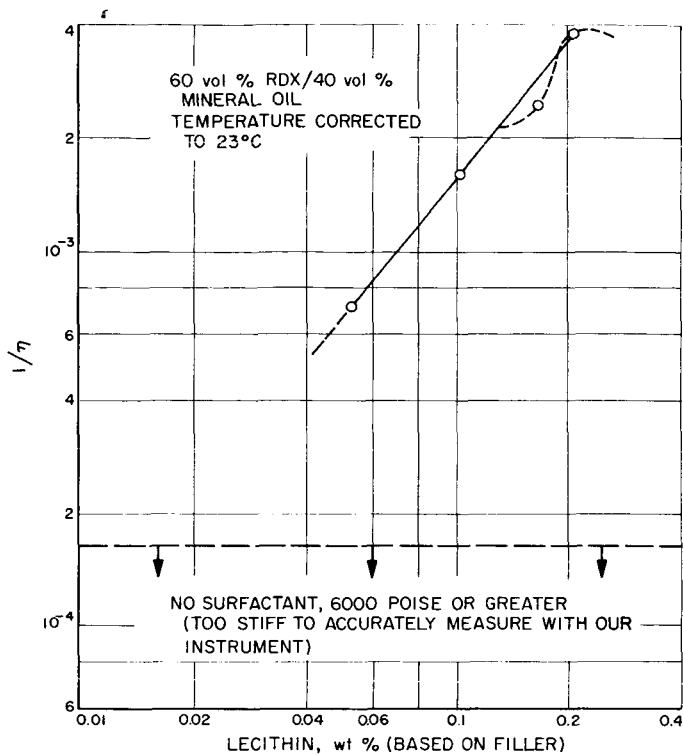


Fig. 5. Effectiveness curve  $1/\eta$  of asolectin on RDX in mineral oil

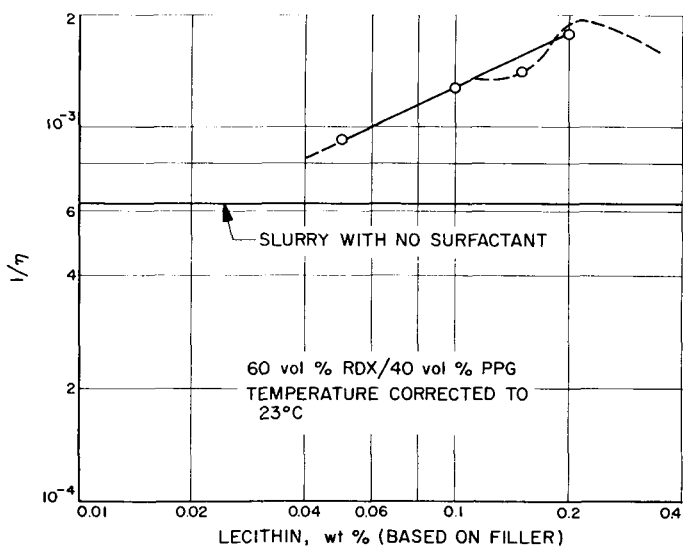


Fig. 6. Effectiveness curve  $1/\eta$  of asolectin on RDX in POPG

allow sufficient number of surfactant concentrations to determine whether the fluidity peaked then declined again as did the effectiveness curves on other materials in previous reports. The above inconvenience plus the hazard which necessitates the use of the parallel plate viscometer rather than the glass plate technique also ex-

plains the comparatively few points on the curves. Nevertheless, it is clearly shown that for all three systems, HMX in mineral oil, and RDX in mineral oil and in POPG, asolectin is an effective fluidity inductant. Furthermore, the preliminary pip as reported in QSR 38-13 appears to be present for these two fillers (also the dashed portion of all three curves).

*b. Fit of viscosity data to master curve.* It was reported in Refs. 4 and 5 and QSR 38-12 and 38-13 that slurries of surfactant-coated particles studied always have a lower relative viscosity than slurries of uncoated particles. Fig. 7 indicates that this is equally true for the

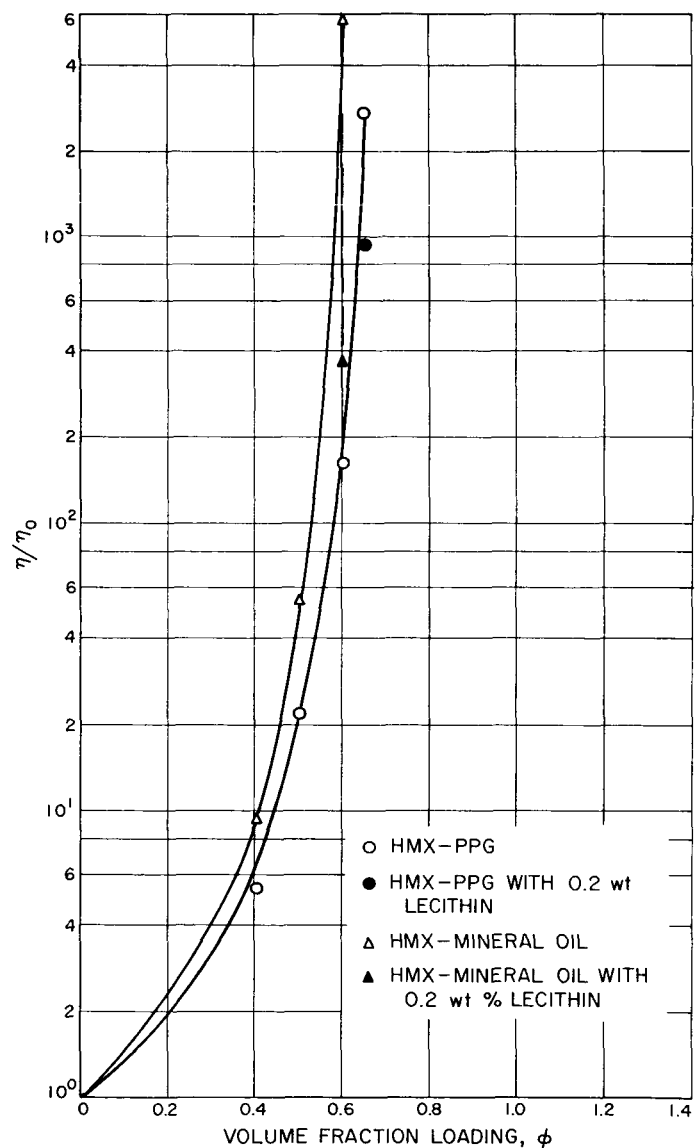


Fig. 7. Relative viscosity versus volume fraction loading for four systems

organic crystal HMX (the filled symbols are the coated mixes). It can also be noted from Fig. 7 that of the two systems studied, HMX in mineral oil and HMX in POPG, each describes a unique curve. If the same data is plotted as  $\phi/\phi_m$  versus relative viscosity (where  $\phi$  is the volume fraction of solids, and  $\phi_m$  is the maximum volume fraction of solids possible in a given system), using the assumed  $\phi_m$ 's discussed in the introduction, one achieves the plot shown in Fig. 8. The solid line is the master curve and fits the equation

$$\frac{\eta}{\eta_0} = \left(1 - \frac{\phi}{\phi_m}\right)^{-2.5}$$

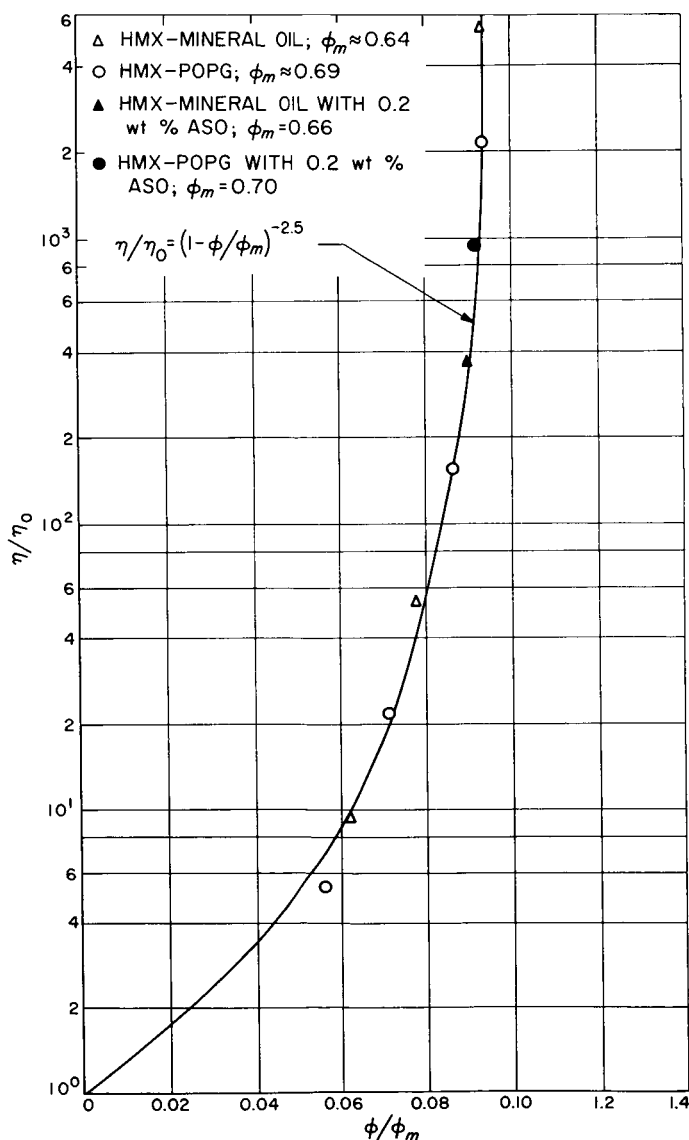


Fig. 8. Relative viscosity versus relative volume fraction loading of four systems

As can be seen, the fit of the new data is excellent. Furthermore, it is estimated that the fit will remain good when the corrected values of  $\phi_m$  are determined. This is shown by the symbols on the plot. These large symbols represent the horizontal range of deviation that an error of up to 2% would yield. Fig. 9 shows all data thus far obtained (including all from previous reports as well as this report), fit to the master curve. (The outlying AP is still attributed to the slight solubility of the finely ground AP in the suspending media and to the variable and rather uncontrollable amount of surface moisture on this

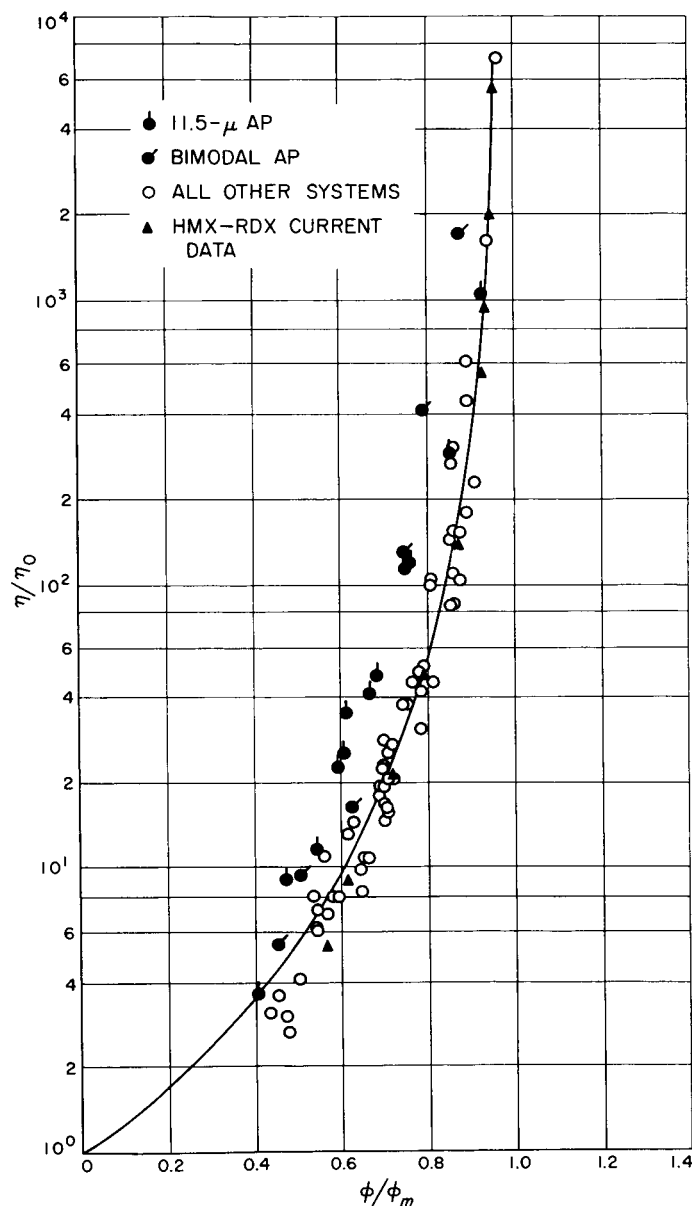


Fig. 9. Master curve of  $\frac{\eta}{\eta_0} = \left(1 - \frac{\phi}{\phi_m}\right)^{-2.5}$

same AP.) Further data at low volume fraction loading is being obtained but is not yet ready for reporting.

*c. Effect of asolectin on tensile properties of AP-Al-polyurethane propellant.* It was previously determined

(QSR 38-13) that asolectin reacts with the isocyanate in a polyurethane system. For that reason it is necessary to increase the isocyanate to hydroxyl ratio in order to effect a cure. Naturally any change in the binder parameters makes it necessary to optimize the cure time as compared to the tensile properties. This is shown in Figs. 10 and 11.

It becomes obvious when studying Figs. 10 and 11 that the addition of asolectin to the mix, using an NCO/OH ratio of 1.12 and  $\text{OH}_{\text{triol}}/\text{OH}$  of 0.130 (filled triangles), results in reduced tensile strength as well as reduced modulus. This becomes especially pronounced with increase in cure time, suggesting that the aging properties

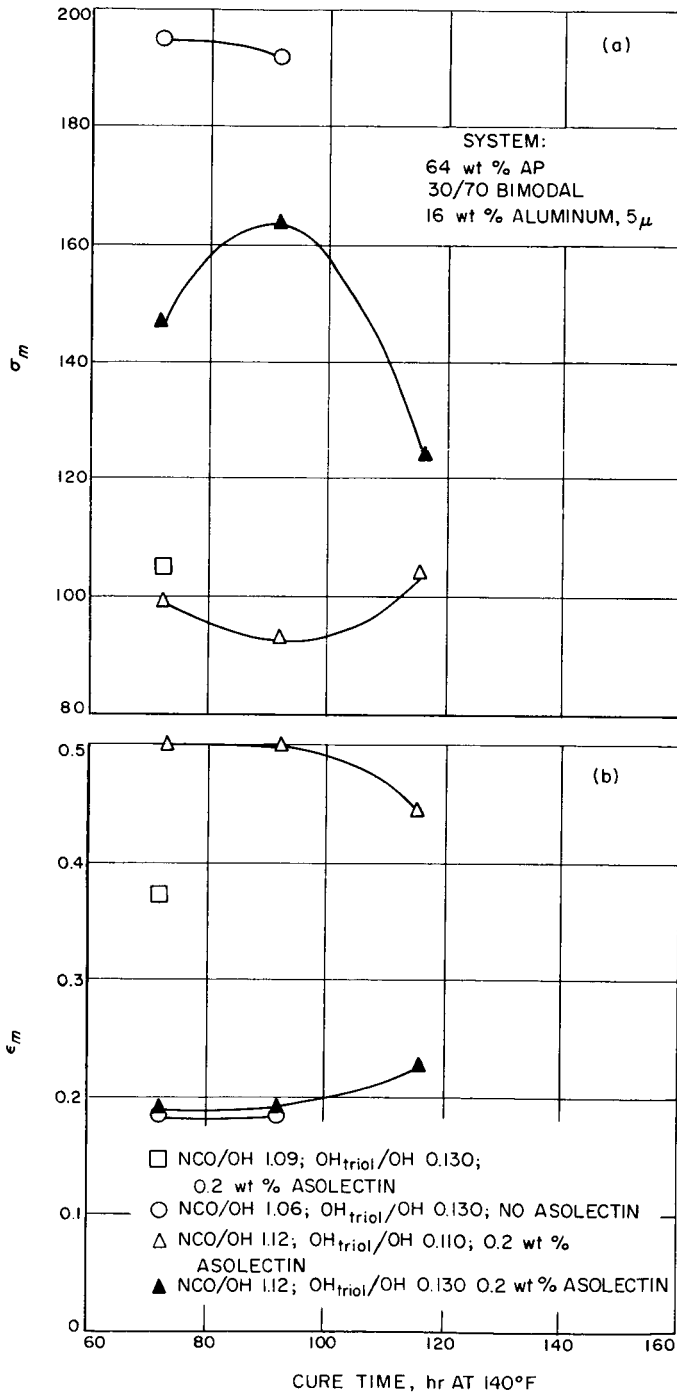


Fig. 10.  $\sigma_m$  versus cure time and  $\epsilon_m$  versus cure time for four binder systems

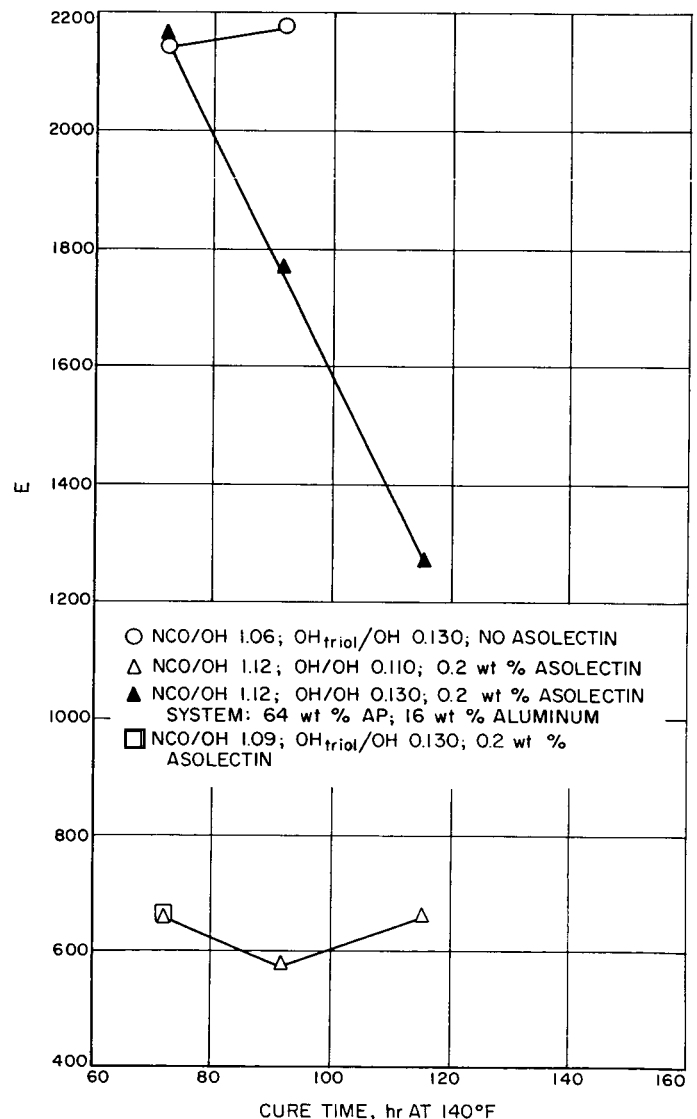


Fig. 11. Modulus  $E$  versus cure time for four binder systems

may be very poor. Furthermore, a reduction of the cross-linker to 0.110 as displayed in the open triangles results in additional decrease in tensile strength and modulus. In this case, however, the elongation is substantially increased at the optimum cure time.

Another method of plotting the data, making it possible to study the three factors—modulus, tensile strength, and elongation—on the same plot, is illustrated in Fig. 12. Here  $\log \sigma_m/E$  vs  $\log \epsilon_m$  is plotted. All the systems plotted in Figs. 10 and 11 plus JPL Syncom propellant appear to lie on a single straight line curve, in agreement with the data of Fedors and Landel (QSR 38-14). This would seem to indicate that a change in any one parameter, for example  $\epsilon_m$ , either by change of binder ratios or by change of volume percent loading, would change the other two parameters  $E$  and  $\sigma_m$  to some proportioned values located on this curve.

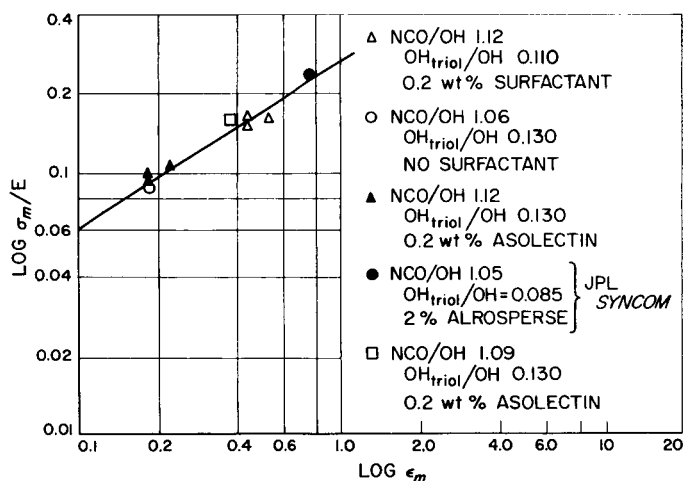


Fig. 12.  $\log \sigma_m/E$  versus  $\log \epsilon$  for five binder systems

The question now is, what parameter would be changed if one were successful in changing the binder-filler bond? Would the point representing some propellant system shift horizontally parallel to the  $x$  axis, vertically along the  $y$  axis, or merely slide up and down the straight line curve?

Obviously, some means of separating the binder component of the total rheological behaviour from the interfacial, or reinforcing component, is drastically needed at this time. If one had a mathematical relation between  $E$ , the modulus of the filled system, and  $E_0$ , the modulus of the binder, then for a given binder-filler system, one would be in a position to see changes in interfacial forces.

Therefore, it seems expedient to devise experiments employing different types of filler and binder parameters so that one might find some empirical  $E/E_0$  relationship. These experiments are in progress, and the results will be reported in a later QSR.

In the meantime, an attempt to find a reactive wetting agent continues. An hydroxylated lecithin with OH groups substituted at double bond sites in the fatty acid chain of the phospholipid molecule will be used in a propellant mix. These OH groups should be free to react with the binder and achieve a tight interfacial bond.

**d. Burning rate of highly loaded propellant.** The first steps have been taken in the evaluation of the strand burning rate of high solids loaded propellant and propellant containing small quantities of prilled oxidizer. The burning rate for an 87% solid polyurethane (71% ammonium perchlorate of a 30/70 bimodal blend of 12- and 101- $\mu$  D; 16% aluminum of 5- $\mu$  D) has been compared with the burning rate of 80% solid propellant (64% bimodal blend and 16% aluminum, same sizes as above). The strands used were standard  $\frac{1}{4} \times \frac{1}{4} \times 5$  in. specimens, restricted and wired. Fig. 13 compares the results over a pressure range of 50 to 2000 psi. Clearly, the burning rate of the 87% solid far exceeds that of the analogous 80% propellant. The results of highly (volume) loaded propellant containing porous prills will be reported later. However, it is postulated that the prills, introducing a very greatly increased burning surface, will result in even higher burning rates. The objectives of present experimentation are to obtain prilled oxidizer that has been cocrystallized with a modifier and to tailor burning rates to an even greater extent.

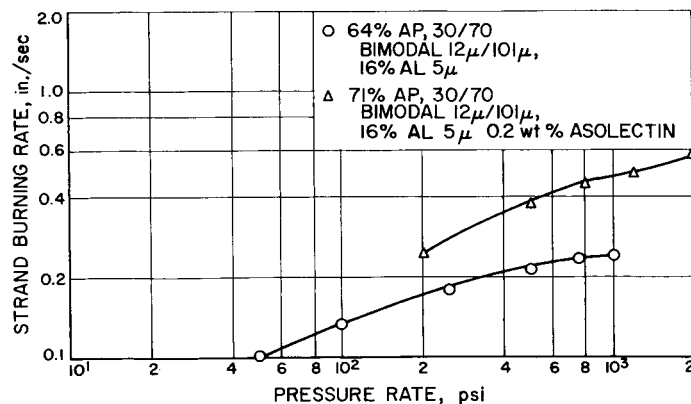


Fig. 13. Comparison of burning rate of 87% loaded propellant with 80% loaded propellant

## C. Ultimate Properties of Crosslinked Amorphous Gum Elastomers

R. F. Fedors and R. F. Landel

It has been shown that the ultimate properties of a noncrystalline gum rubber at constant crosslink density measured as a function of the test temperature and the strain rate can be characterized by a time and temperature independent failure envelope (Ref. 6). This envelope is generated by plotting in log-log coordinates  $\sigma_b T_0/T$  versus  $\epsilon_b$  where  $\sigma_b$  is the stress-at-break based on the initial cross-sectional area,  $T_0/T$  is a temperature reduction factor, and  $\epsilon_b$  is the strain-at-break.

When the number of effective network chains  $\nu_e$ , or the equilibrium modulus  $E_e$ , is varied for a particular rubber, a series of failure envelopes, which are similar in shape, can be generated. Based on preliminary data obtained with a peroxide-cured styrene-butadiene rubber (SBR) it appeared that the effect of varying  $\nu_e$  could be taken into account by normalizing  $\sigma_b$  to unit  $\nu_e$  (Ref. 7). More recently it was demonstrated that this normalization procedure enabled the high temperature portions of the failure envelopes of some fourteen systems to be superposed (Ref. 8). The factor  $T_0/T$  was replaced by the factor  $(T_g + 100)/T$ , where  $T_g$  is the glass transition temperature, since ultimate property data obtained from elastomers having different  $T_g$  values were employed. It should be emphasized that it does not appear possible by means of this normalization scheme to superpose the entire failure envelope corresponding to each value of  $\nu_e$  or  $E_e$ . Rather, only the high temperature portions of the envelopes superpose to describe a "universal" curve which is termed the common response curve. The remainder of each envelope diverges from the common response, and this effect gives rise to the occurrence of branches originating from the common response curve. The existence of these branches is believed to be associated with finite extensibility of the network chains.

Smith (Ref. 9) has recently proposed an alternative method of normalizing ultimate property data. Briefly, Smith proposed a log-log plot of  $\lambda_b \sigma_b T_0/T$  versus  $\epsilon_b E_e T_0/T$ , where  $\lambda_b$  is the extension ratio at break, and  $E_e$  is an equilibrium modulus defined by the relation  $\sigma \lambda = E_e \epsilon$ . If no change in volume occurs on extension, the factor  $\lambda_b \sigma_b$  represents the true stress based on the actual cross-sectional area at break. This reduction scheme was reported to have superposed the failure en-

velope for a series of viton gum rubbers when  $E_e$  was varied by a factor of about ten (Ref. 9).

The importance of the existence of the failure envelope and its dependence on  $\nu_e$  or  $E_e$  resides in the fact that it becomes possible to represent very simply the rupture behavior of a rubber under a vast variety of test conditions. Moreover, to the extent that the reduced failure envelope is independent of the chemical nature of the rubber, it becomes possible to describe the general features of rupture of a rubber network.

Hence it is of considerable interest to compare the rival schemes which have been proposed for the reduction of ultimate property data. Recently, limited but independent data have become available which will be used here to test the ability of the alternative methods to represent the experimental data.

Recently Dudek<sup>1</sup> measured the ultimate properties of gum SBR and ethylene propylene rubber (EPR) of different  $\nu_e$  values at several rates and temperatures. For the SBR rubber,  $\nu_e$ , as determined by swelling in benzene, taking  $\mu = 0.34$ , varied from 6.8 to 148  $\mu\text{mole}/\text{cm}^3$ , while for EPR,  $\nu_e$ , calculated from data obtained with stress-strain experiments on swollen specimens, varied from 0.435 to 87  $\mu\text{mole}/\text{cc}$ . The ultimate properties were measured on ring specimens at 25 and at 78°C, using strain rates of 0.060 and 1.25  $\text{min}^{-1}$  at each temperature. Although these results are insufficient to define the entire failure envelope for each  $\nu_e$  value, it is possible to describe portions of each envelope. It is evident that if the entire envelope will superpose when a particular normalization scheme is employed, then portions of the envelope will of necessity also superpose. Hence, while more complete data would be very desirable, the present data are believed sufficient for the present purposes.

In Fig. 14 the ultimate property data obtained with SBR rubber are plotted according to the reduction scheme of Smith (Ref. 9) with the exception that the abscissa contains the term  $\nu_e$  rather than  $E_e$ . For the data of Dudek, at least, this substitution introduces no appreciable error since each envelope is shifted by approximately a constant factor and hence the relative position of each envelope is essentially unchanged. The curves in Fig. 14 represent portions of the failure envelope for each of the indicated  $\nu_e$  values. According to Smith, this coordinate system should superpose the envelopes. It may be observed that there is no superposition and further-

<sup>1</sup>Dudek, T., private communication.

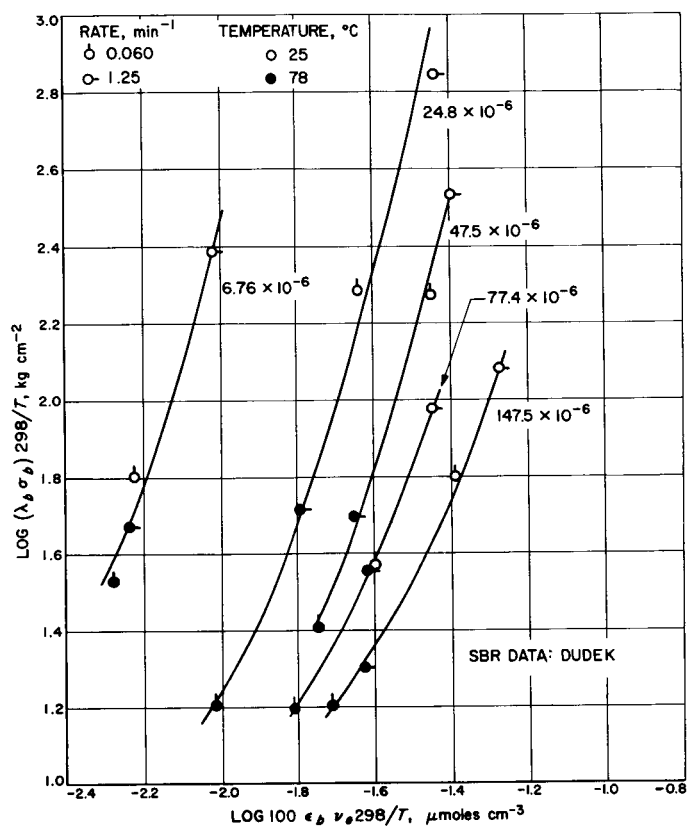


Fig. 14. Ultimate properties of SBR gum vulcanizates measured at the indicated strain rates and temperatures for five crosslink densities

more, the envelopes are displaced so that they intersect an arbitrarily chosen value of the ordinate, at values of the abscissa which increase with increasing  $\nu_e$ . In Fig. 15<sup>2</sup> the data are replotted according to the alternative reduction scheme in which  $\sigma_b$  is normalized to unit  $\nu_e$ . Comparison of Figs. 14 and 15 indicates that the latter reduction scheme provides a better description of the experimental data.

A similar comparison is made in Figs. 16 and 17 for the EPR data. In the Smith plot (Fig. 16), the divergence between the envelopes obtained at constant  $\nu_e$  is even more serious than that observed with SBR (Fig. 15). The interval on the abscissa between the envelopes representing the lowest and the highest value of  $\nu_e$  is about three decades. It is also evident that, as was observed for SBR, the envelopes for EPR intersect an arbitrarily chosen value of the ordinate at values of  $\log 100 \epsilon_b \nu_e T_0/T$  which increase with  $\nu_e$ . Fig. 17 shows the EPR data when  $\sigma_b$  is normalized to unit  $\nu_e$ . It is evident that the correlation

<sup>2</sup>Since  $\sigma_b$  is usually given in psi and  $\nu_e$  in moles/cm<sup>3</sup>, the mixed dimensions are retained here for the convenience of the reader.

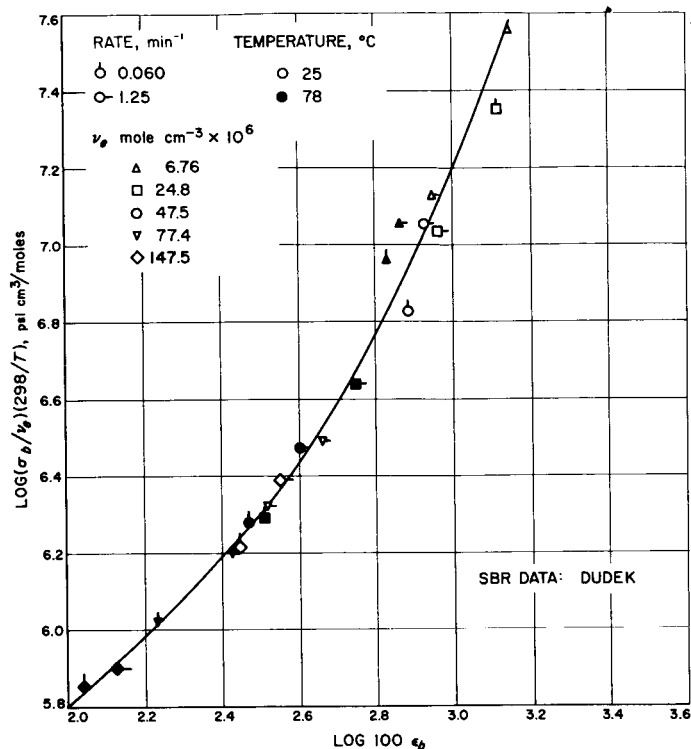


Fig. 15. Data of Fig. 14 plotted according to the reduction scheme of Landel and Fedors (Ref. 8).

here is not as good as that obtained with the SBR data. In Fig. 18, the ultimate property data obtained with both SBR and EPR are compared with  $\sigma_b$  normalized to unit  $\nu_e$ . The dashed line in the figure represents the reduced failure envelope taken from Ref. 8. Also shown in the figure are several data points obtained with poly (vinyl-ethyl ether) gum vulcanizates (Ref. 10).  $T_0$  for this latter rubber was assumed to be  $-65^\circ\text{C}$ .

Novikov, et al. (Refs. 11, 12) have recently studied the effect of peroxide and amine curing agents on the ultimate properties of a viton elastomer. Although they were primarily concerned with the effects of compounding and vulcanization variables on the physical properties of the resultant vulcanizates, sufficient data to construct a reduced failure envelope were reported. Values of  $\nu_e$  were estimated from equilibrium swelling in acetone using a  $\mu$  value determined from osmotic pressure measurements.

In Fig. 19, the data obtained (Refs. 11 and 12) with viton are shown according to the Smith reduction scheme. In Fig. 20,  $\sigma_b$  is normalized to unit  $\nu_e$ , and the dashed line indicates the position of the failure envelope obtained by Smith for a viton elastomer with  $\nu_e = 114 \mu\text{moles/cc}$  of rubber (Ref. 13). However, an arbitrary shift along the

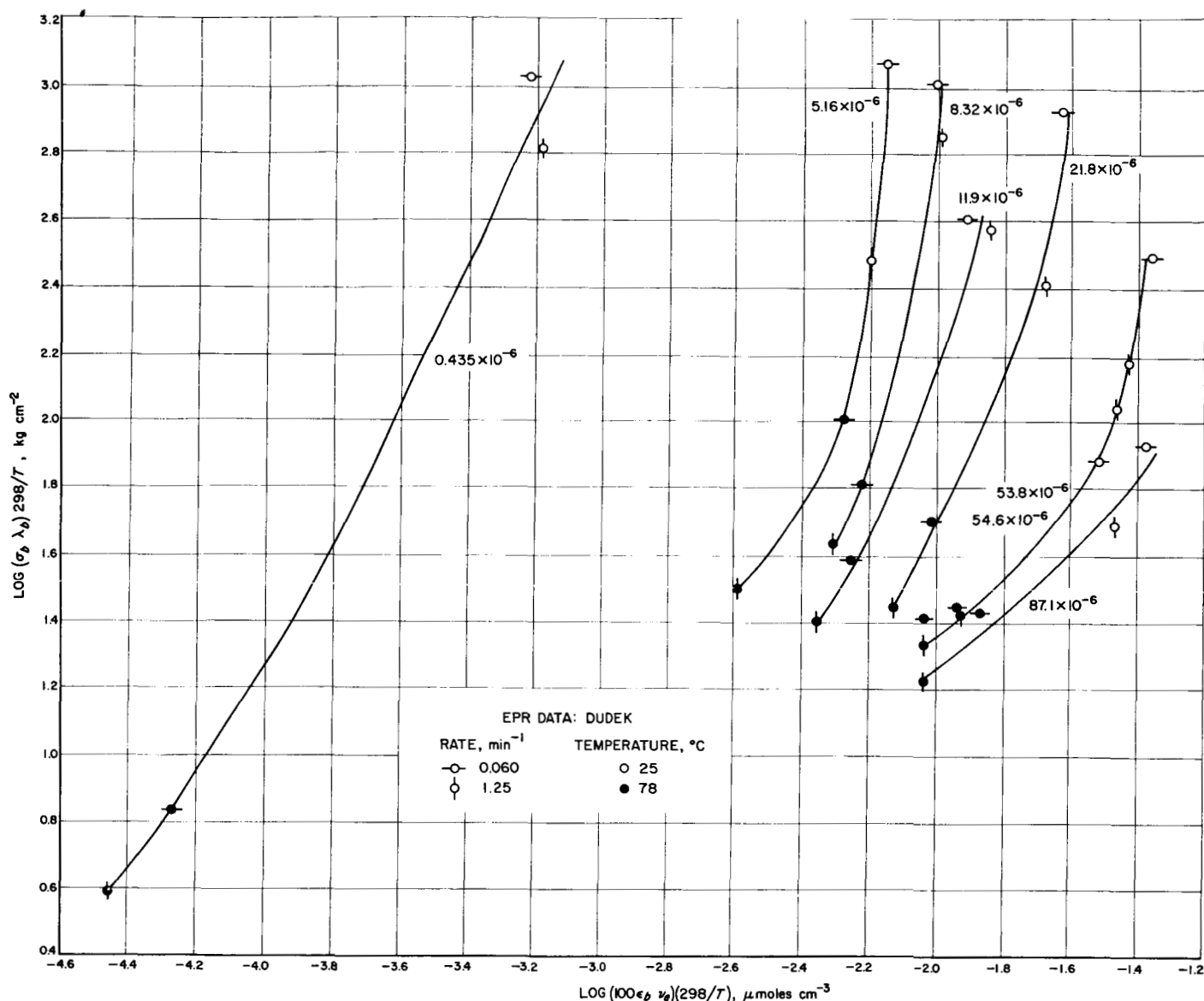


Fig. 16. Ultimate properties of EPR gum vulcanizates measured at the indicated strain rates and temperatures for eight crosslink densities

ordinate of 0.8 log units was required to obtain the superposition of the two sets of data shown in the figure. A possible explanation for the necessity of shifting can be related to the apparently high values of the molecular weight between cross links  $M_c$ , reported by Novikov, which implies that the value of  $\mu$  for the system viton-acetone, used by these workers, is excessively high. For an  $M_c$  of 410,000 gm mole<sup>-1</sup>, the reported sol fraction is only 8.6%. These are not compatible numbers for reasonable values of the molecular weight of the primary molecules. As a first approximation of the magnitudes involved, at constant sol fraction,  $\nu_e$  calculated from Novikov's data is a factor 4 smaller than  $\nu_e$  reported by Smith (Ref. 13).

If the reduction scheme of Smith were completely general, then  $\lambda_b \sigma_b T_0/T$  would be a function of the product  $\epsilon_b E_b T_0/T$ . No other parameters would be necessary to describe the master failure envelope. Hence,

$$\lambda_b \sigma_b T_0/T = g(\epsilon_b E_b T_0/T) \quad (1)$$

The important point to notice is that neither  $\epsilon_b$  nor  $E_b$  can occur alone in  $g$ . This requirement can readily be demonstrated as follows: for an arbitrarily chosen value of  $\lambda_b \sigma_b T_0/T = c$ , consider the envelopes obtained from two rubbers having moduli of  $E_{e1}$  and  $E_{e2}$  where  $E_{e1} = \alpha E_{e2}$ ,  $\alpha = \text{constant}$ . Corresponding to the value of  $c$ , there will be two values of  $\epsilon_b$ ,  $\epsilon_{b1}$  and  $\epsilon_{b2}$  where

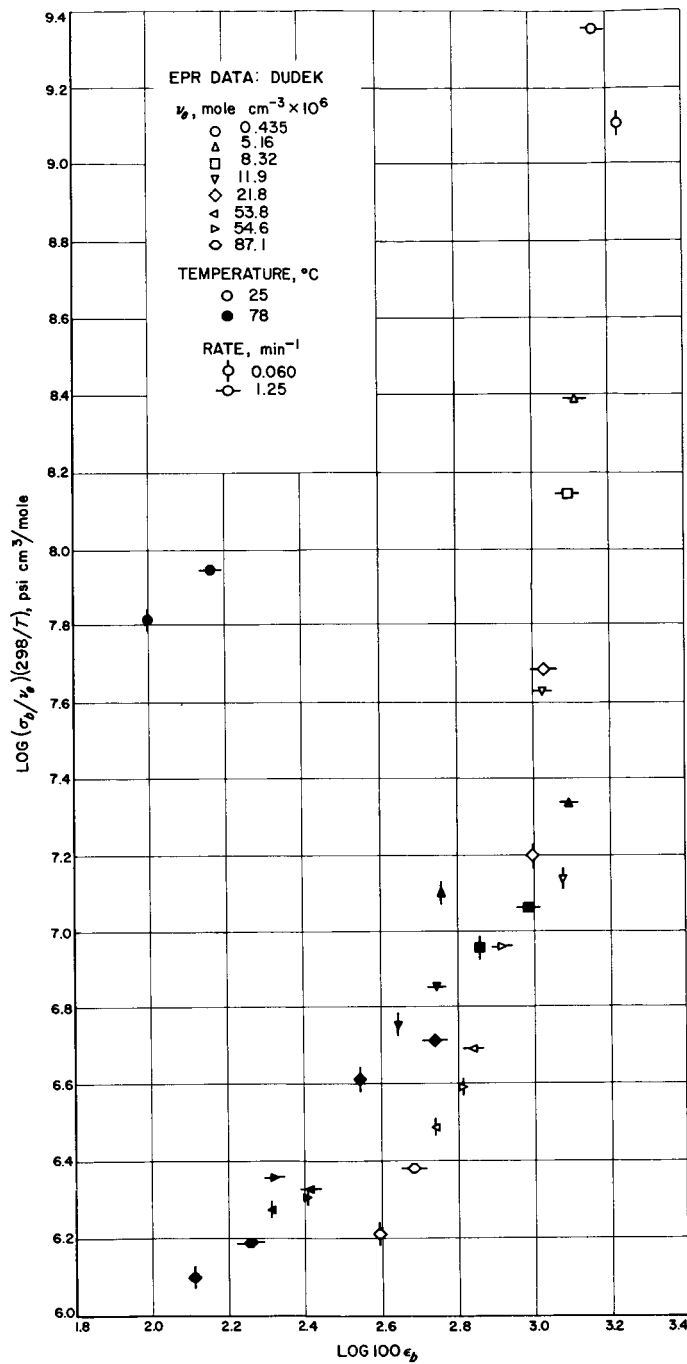


**Fig. 17. Data of Fig. 16 plotted according to the reduction scheme of Landel and Fedors (Ref. 8)**

$\epsilon_{b1} = \beta \epsilon_{b2}$ ,  $\beta = \text{constant}$ . Hence, Eq. (1) can be written as

$$\lambda_b \sigma_b T_0/T = c = g(\epsilon_{b2} E_{e2} T_0/T) = g(\alpha \beta \epsilon_{b2} E_{e2} T_0/T) \quad (2)$$

Only when  $\epsilon_b$  and  $E_e$  occur as the product can the constants  $\alpha$  and  $\beta$  be factored. Furthermore, superposition

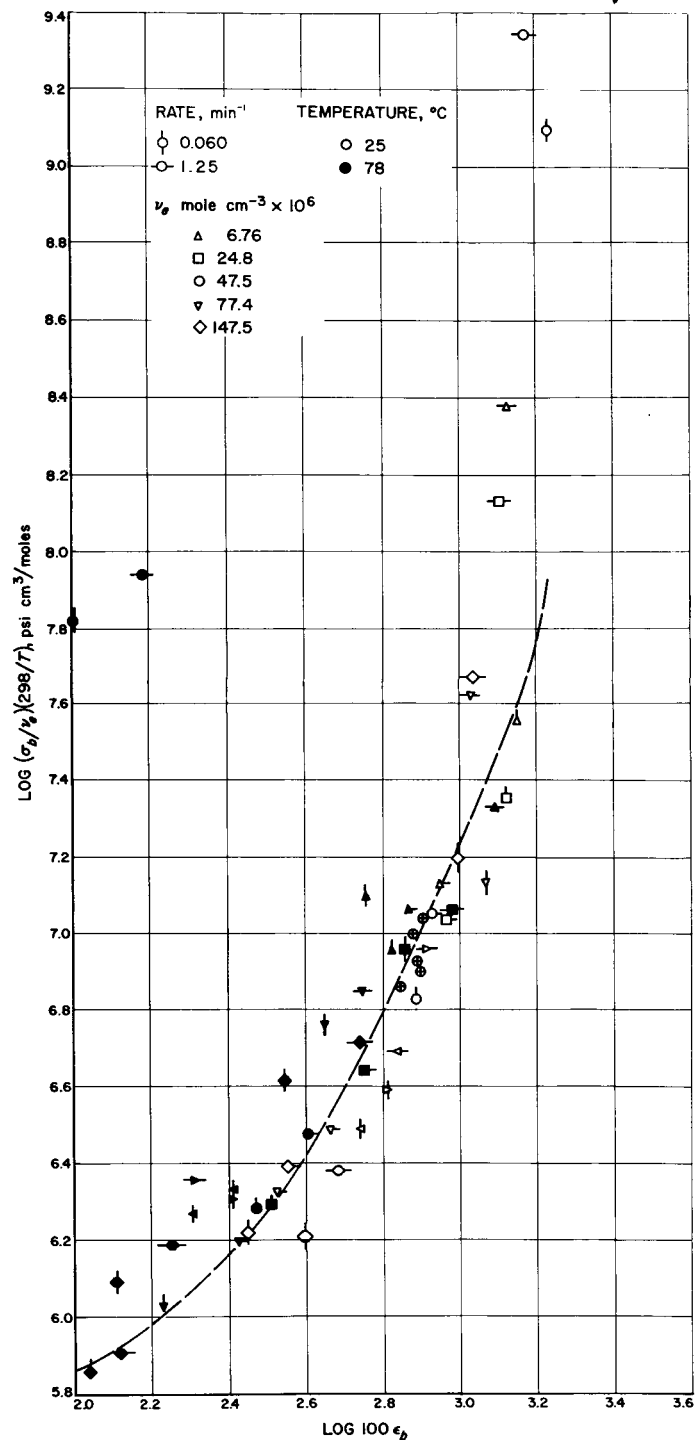


**Fig. 18. Comparison of the ultimate properties of SBR and EPR (Ref. 8, Figs. 15 and 17). Also shown are several points for a methyl ether gum**

of the envelopes requires that  $\alpha\beta = 1$ , which implies that

$$\epsilon_b = T \text{ const } / T_0 E_e \quad (3)$$

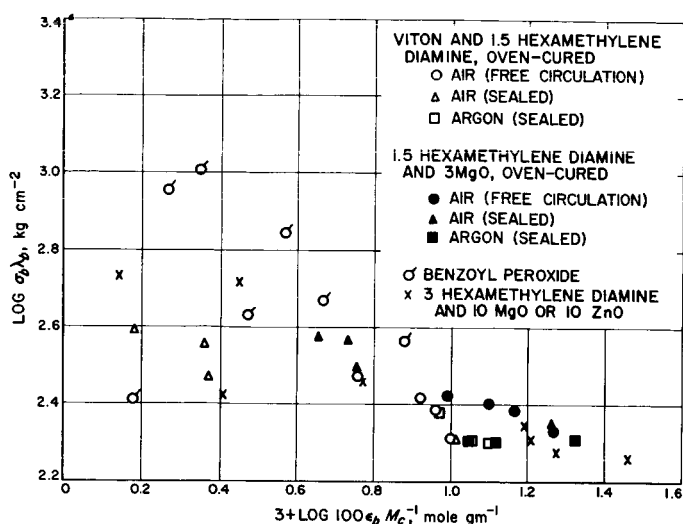


Fig. 19. Ultimate properties of viton vulcanizates, using  $M_c^{-1}$  as a measure of equilibrium modulus  $E_e$

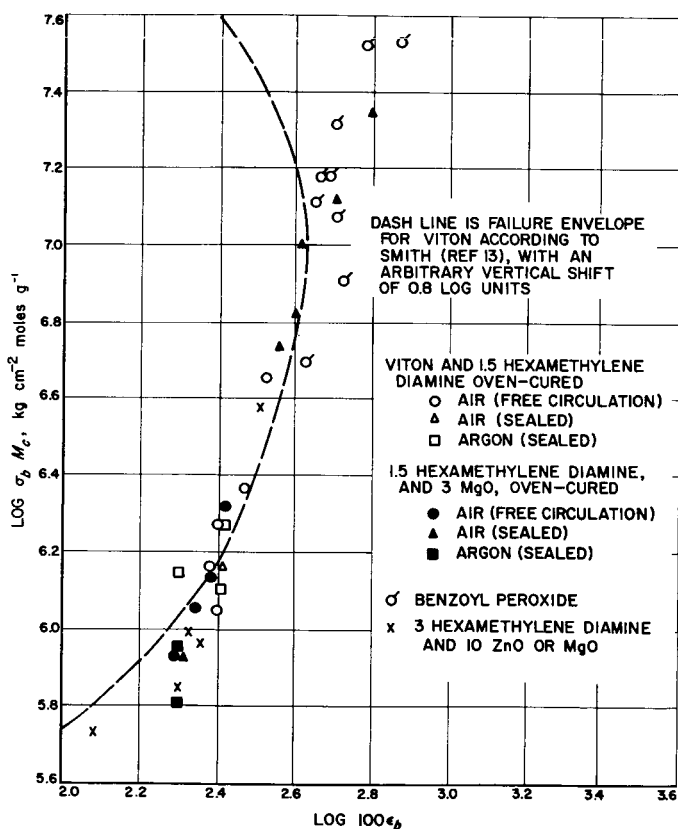


Fig. 20. Data of Fig. 19 plotted according to the reduction scheme of Landel and Fedors (Ref. 8)

i.e., at constant  $\lambda_b \sigma_b T_0/T$ ,  $\epsilon_b$  is inversely proportional to  $E_e$  at constant  $T$ . For viton rubber, Smith reported that at a value of  $\lambda_b \sigma_b = 1.6 \times 10^4$  psi,  $\epsilon_b$  reached a maximum

which was inversely proportional to  $E_e$ . However, Eq. (3) requires proportionality for all values of  $\lambda_b \sigma_b$ , not only at the maximum in  $\epsilon_b$ .

It has been pointed out that when the test rate is sufficiently slow or the test temperature sufficiently high, the failure envelope coincides with the stress-strain curve (Refs. 8, 14). Therefore under these experimental conditions, Eq. (1) must reduce to the stress-strain curve for the rubber. However, theoretical and empirical functions, for example, the kinetic theory expression and the MRS equation (Ref. 15), which are used to describe the form of the stress-strain relationships, can be written as

$$\lambda \sigma T_0/T = E_e f_1(\epsilon) T_0/T \quad (4)$$

Eqs. (1) and (2) will reduce to the same form when  $\lambda \sigma$  is a linear function of  $E_e \epsilon$  (modified Hook's law). Experimental results from peroxide-cured SBR indicate that the stress-strain curve coincides with the failure envelope for  $\epsilon_b$  values even where a linear relationship ceases to be a good approximation.

On the other hand, assume that the failure envelope can be described by an equation of the form

$$\lambda_b \sigma_b T_0/T = \epsilon_b E_e f(\epsilon_b) T_0/T \quad (5)$$

which is equivalent to Eq. (4). For any arbitrarily selected value of  $\lambda_b \sigma_b T_0/T$  consider two envelopes characterized by  $\epsilon_{b1}$ ,  $E_{e1}$  and  $\epsilon_{b2}$ ,  $E_{e2}$ . Then Eq. (5) can be written as

$$\begin{aligned} \log \epsilon_{b1} E_{e1} T_0/T - \log \epsilon_{b2} E_{e2} T_0/T \\ = \log f(\epsilon_{b2}) - \log f(\epsilon_{b1}) \end{aligned} \quad (6)$$

Superposition of the two envelopes requires that  $f(\epsilon_{b2}) = f(\epsilon_{b1})$ . Hence envelopes which can be represented by Eq. (5) will superpose according to the Smith reduction scheme only when  $f$  is independent of  $\epsilon_b$ , i.e., only when  $\lambda_b \sigma_b T_0/T$  is a linear function of  $E_e \epsilon_b T_0/T$ . On the other hand, if it is assumed that  $f$  is a function of  $\epsilon_b$ , then the failure envelopes will not superpose, and hence it may be supposed that  $\epsilon_{b2} E_{e2} > \epsilon_{b1} E_{e1}$  or  $\epsilon_{b2} E_{e2} = \alpha \epsilon_{b1} E_{e1}$ , where  $\alpha > 1$ . For a constant value of the ordinate

$$\epsilon_{b1} E_{e1} T_0/T f(\epsilon_{b1}) = \alpha \epsilon_{b1} E_{e1} f(\epsilon_{b2}) T_0/T \quad (7)$$

or

$$f(\epsilon_{b1}) > f(\epsilon_{b2}) \quad (8)$$

Eq. (8) implies that  $\epsilon_{b1} > \epsilon_{b2}$  if  $f$  is a monotonically increasing function. Under these conditions when  $\epsilon_{b1} E_{e2} > \epsilon_{b2} E_{e1}$  then  $E_{e2} > E_{e1}$ , or the individual envelopes are displaced to the right (to higher values of  $\epsilon_b E_e$ ) as  $E_e$  increases. It has been pointed out above that the envelopes for both SBR and EPR obtained at varying  $\nu_e$  behave in this manner (Figs. 14 and 16).

As another illustration of this behavior, in Fig. 20 the MRS equation is plotted according to the reduction scheme of Smith for four values of  $E_e$ . In the MRS equation,  $f(\epsilon)$  is given by

$$f(\epsilon) = \lambda^{-1} \exp A(\lambda - 1/\lambda) \quad (9)$$

where  $A$  is a constant for which the value 0.40 has been assumed for the curves shown in Fig. 21. For this  $f(\epsilon)$ , the inequality shown in Eq. (8) implies  $\epsilon_{b1} > \epsilon_{b2}$ . Also shown as the dashed curves are some experimental failure envelopes taken from a recent publication of Smith (Ref. 14). The similarity in shape and position of the experimental envelopes to those derived on the basis of an  $f(\epsilon)$  given by Eq. (9) is indeed striking. And for these envelopes at least, Eq. (4) provides as good a representation of the experimental data as does Eq. (1).

The preferred reduction scheme where  $\sigma_b$  is normalized to unit  $\nu_e$  is not as satisfying as it might be, since the low temperature portions of individual failure envelope branches representing varying  $\nu_e$  do not superpose. The reasons for the existence of the branches which originate on the common response curve is not well understood; they appear to be related to finite extensibility of the network chain. It is apparent that a function of  $\nu_e$  is

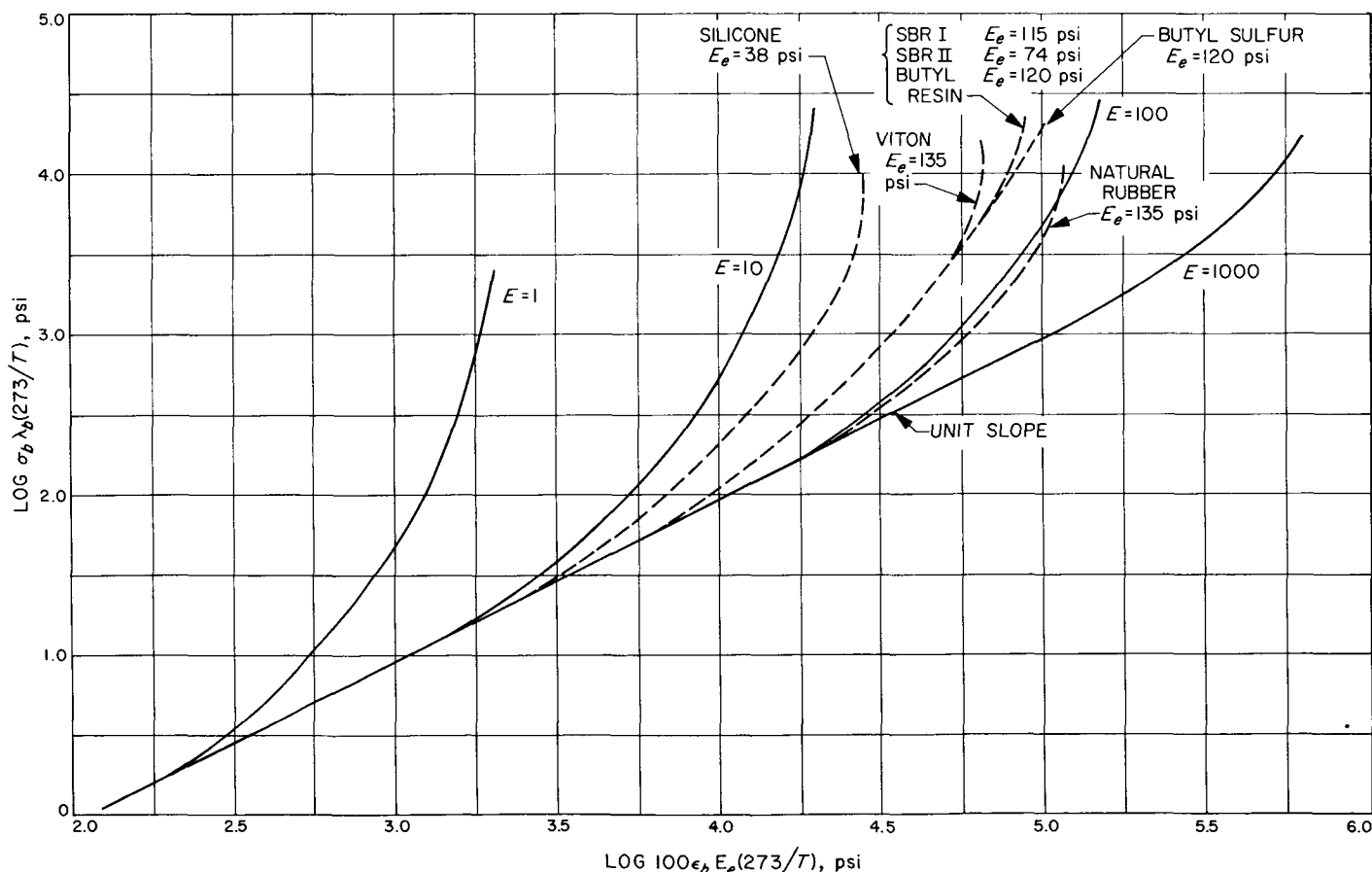


Fig. 21. Comparison of the MRS equation,  $A = 0.40$ , (solid lines) with experimental failure envelopes reported by Smith (Ref. 15), plotted according to the reduction scheme of Smith (Ref. 9)

needed in order to superpose the branches. However, it has been demonstrated that the function defined by Eq. (1) is apparently too strongly dependent on  $v_e$  and the function defined by Eq. (5) too weakly dependent on  $v_e$  to effect this superposition. At the present time, however, normalization of  $\sigma_b$  to unit  $v_e$  has the ability to correlate more ultimate property data for more diverse systems than has heretofore been possible.

## D. Continuous Media Theory Applied to Viscoelastic Strain Analyses, V

A. San Miguel

The objectives of this study (see previous QSR's) have been to reinterpret concepts found in the general literature in terms of solid propellant mechanical property technology. This study has led to the development of the multiaxial inflated cylinder test as well as to the emphasis of continuous media theory in lieu of the dashpot theory of linear viscoelasticity. The immediate interest has been in characterizing a so-called strain energy function in a manner unorthodox to the "classical" concept.

One problem associated with the inflated cylinder test, as well as with the so-called strain energy function, is that other multiaxial tests must be performed before the validity of this approach can be established. A relatively simple multiaxial experiment is that of a tension-tension biaxial sheet test. In this report a description of one such biaxial tester is given, as well as the techniques necessary to reduce the measured stress states. Finally, the strain energy mode and magnitude is computed and compared with the strain energy mode and magnitude obtained from the inflated cylinder test.

### 1. The Biaxial Tensile Test

One reason to develop multiaxial experiments is that the multidimensional theory of continuous media requires a measurement of at least two simultaneous stresses in conjunction with the three principal strains, in a point region. This condition may be satisfied by conducting

homogeneous experiments, i.e., where the stress-strain state of a test structure is the same at all points in the structure and curved or straight lines deform into curved or straight lines. The inflated cylinder test is an example where homogeneous stresses and strains are found at any particular radial distance. However, the advantage of the inflated cylinder test is that *many* homogeneous stress-strain states can be examined simultaneously at every internal pressure level. On the other hand, a presumably simpler multiaxial test would be that of a tension-tension state in a sheet or plate of material.

A biaxial tensile test consists of applying two principal tension stresses to a sheet or plate of material. The homogeneous strains are then measured in some fashion together with the thickness changes. This multiaxial test has been used by prominent investigators such as Treloar (Ref. 16) in establishing photoelastic stress-optic phenomena and Rivlin (Ref. 17) in his experimental studies of the strain energy function of a rubber. Blatz and Ko (Ref. 18) have also done some experimental studies with polyurethane rubber and foam with the objective of eventually studying solid propellant.

A biaxial tensile test at first appears to be simple to construct and implement properly. To the contrary, this test is as difficult to construct properly as any of the multiaxial tests. There are no exact methods to measure the absolute magnitudes of the biaxial principal stresses in the center of the sheet. A technique to measure approximate principal stresses in the center of a sheet is presented here which is analogous to the effective length approach used to calculate strains in uniaxial testing.

### 2. The Measurement of Stresses

Stress is defined as a force per unit area. Strictly speaking, a vector  $T$  giving the force per unit area over some surface  $S$ , bounding the volume  $V$ , has components of the form

$$T_i = \tau_{ij} v^j \quad (1)$$

In this equation  $\tau_{ij}$  are the components of a tensor and are functions of position and *time* and  $v^j$  are the components of a unit vector  $v$ , normal to the surface under consideration. By restricting ourselves to an experiment where only principal stresses and strains are imposed, the only nonzero stress tensor components are  $\tau_{11}$ ,  $\tau_{22}$  and  $\tau_{33}$ . The basic problem associated with the biaxial sheet test

is to measure  $\tau_{11}$  and  $\tau_{22}$  ( $\tau_{33} = 0$ ) knowing only the boundary loads and the principal strains at the center of the sheet.

The boundary loads on a sheet of material can be measured by any of a number of methods. Rivlin used calibrated springs; Blatz and Ko used rigid boundary load-transferring members in conjunction with a uniaxial tensile machine to measure equal biaxial stresses. Treloar used a string-pulley-weight system. These methods are all experimentally interrelated and are suitable for preliminary studies. Ideally, the experimentalist would want a boundary loading system which was rigid, applied uniform loading to the sheet boundary, compensated cross-strain-caused stretches, imposed nonequal biaxial stresses, and was capable of instantaneous load readout for creep and relaxation testing.

The problem in the sheet tensile test is knowing what *area* the transmitted load is acting upon. Previous investigators have arbitrarily assigned *areas* in their calculations of stress. This would conceivably be proper for ordinary engineering, but not if rigorous theory is to be verified by such experimentation. Rubber sheet experimentation, where strains of the order of 50 to 300% are experienced (Fig. 22), cannot have areas arbitrarily assigned for stress computations. This can easily be verified upon inspection of such a test under polarized light. This is not to say that a homogeneous biaxial stress state does not exist in the center region of the sheet. For this state does, indeed, exist. However, the load distribution pattern away from the center region changes because the sheet no longer has the boundaries of a rectangle. This undesirable boundary effect changes the absolute magnitudes of the principal stresses in the center region as compared to those magnitudes experienced for small strains where rectangular boundary distortions can reasonably be experienced. This problem would become quite evident if this biaxial test were performed on a viscoelastic material such as solid propellant. Hence, some attempt must be made to approximate the stressed area in a rational fashion.

No matter how a sheet is clamped, local stress distributions will exist away from the homogeneously stressed center region. Monch (Ref. 19) has shown, using a stress freezing technique, that for even infinitesimal strain, the experimentalists cannot avoid these stress concentrations; they can only minimize them. Preliminary experimental investigations at this laboratory with low-modulus photoelastic coatings confirm the observations of Monch. This

experimental difficulty is also found in uniaxial tensile testing.

Fig. 22a illustrates the geometry of the tension sheet under consideration. It is readily recognized that the initially square sheet will, in general, deform (or map) into a rectangle (Fig. 22b), depending on which of the applied loads is greater. However, as the loading increases, the over-all geometry actually deviates from a rectangle (Fig. 22c). At the center of the sheet, no deviations from orthogonality can be measured. Hence, the

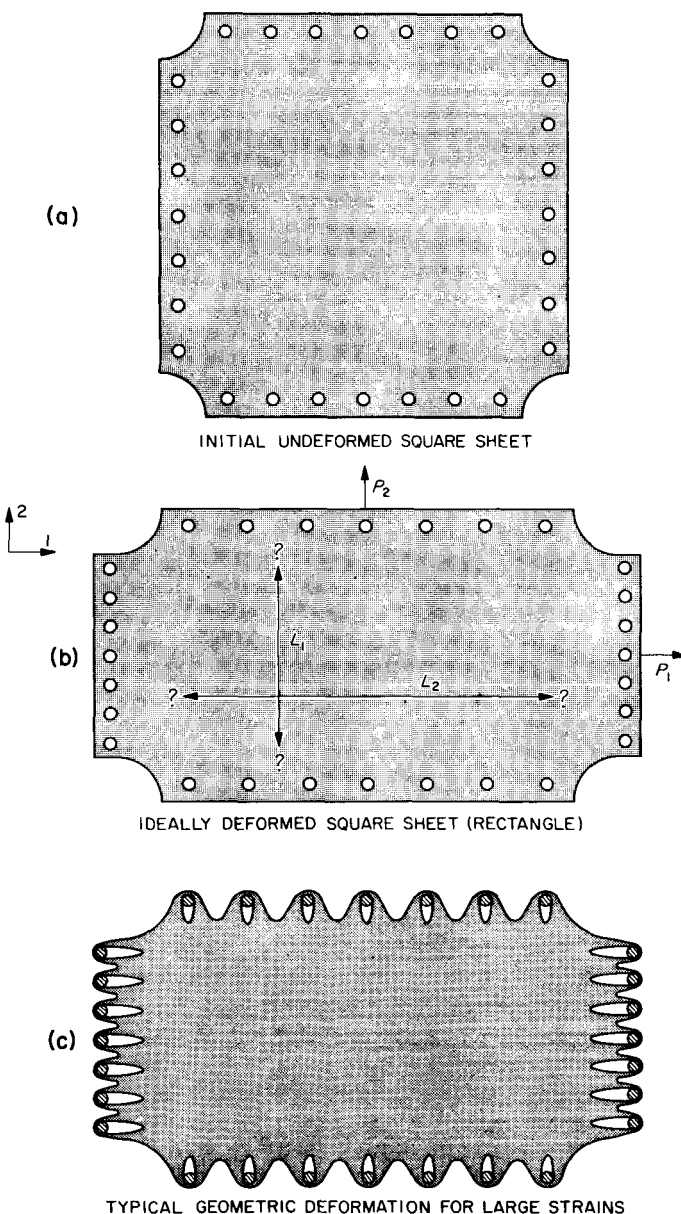


**Fig. 22. Ideal versus actual sheet deformations for large strains**

stress-strain relationship at the center of the sheet can be defined for a linear elastic material as

$$\begin{aligned}\epsilon_{11} &= \frac{\tau_{11}}{E} - \frac{\mu\tau_{22}}{E} \\ \epsilon_{22} &= \frac{\tau_{22}}{E} - \frac{\mu\tau_{11}}{E} \\ \epsilon_{33} &= -\frac{\mu}{E}(\tau_{11} + \tau_{22})\end{aligned}\quad (2)$$

If the elastic material is also incompressible, then

$$(1 + \epsilon_{11})(1 + \epsilon_{22})(1 + \epsilon_{33}) = 1 \quad (3)$$

The loads  $P_1$  and  $P_2$  are directional and are distributed across  $L_1$  and  $L_2$  (Fig. 22b) in some unknown fashion, i.e., the load at the center may be larger than the average load across  $L_1$ . A problem arises in that  $L_1$  and  $L_2$  are unknown. To say that the edges do not carry load would not be precise. Thus, the problem is to estimate the functions  $L_1$  and  $L_2$ . The most obvious, although not precise, relationship would be to postulate that the significant relationship is

$$L_1 = f_1(\epsilon_{22}) \text{ and } L_2 = f_2(\epsilon_{11}) \quad (4)$$

It should be noted that each effective length is a function of both "point region" principal strains as well as the structure geometry.

For expedience, pseudostresses are defined as

$$\sigma_1 = \frac{P_1}{tL_1} \text{ and } \sigma_2 = \frac{P_2}{tL_2} \quad (5)$$

where

$$t = t_0(1 + \epsilon_{33})$$

Now, if experimentally one could measure  $\epsilon_{11}$ ,  $\epsilon_{22}$ ,  $\mu$  and  $E$ , then  $\tau_{11}$  and  $\tau_{22}$  could be computed from Eq. (2) for a linear elastic material. Then assume that the pseudostresses of the entire sheet be equal to the stresses at the center,

$$\tau_{11} = \sigma_1 \quad \tau_{22} = \sigma_2 \quad (6)$$

If one can then measure  $\epsilon_{33}$ , then  $L_1$  and  $L_2$  can be computed from Eq. (5). If the material is incompressible, then Eq. (3) can be used to verify the experimentally obtained  $\epsilon_{33}$ . A plot of  $L_1$  versus  $\epsilon_{22}$  and  $L_2$  versus  $\epsilon_{11}$  (experimentally obtained) would then serve to characterize the relationship between boundary loading and center-of-sheet stress for the particular geometry, loading ratios  $P_1/P_2$ , and the particular biaxial tester including the technique of clamping. Thus, it appears that an experimentally determined effective length can be used to approximate the stress conditions at the center of a sheet. Once determined, this effective length could be used with any material (such as propellant) since the stress state is only a function, not of the material, but of the boundary conditions which are peculiar both to the specimen geometry and also to the testing machine. The linear elastic material used to calibrate the biaxial tensile tester should have a modulus of the same order of magnitude as that of the unknown material to be tested.

### 3. The Measurement of Strains

Previous experimental work with uniaxial tensile bars has shown that the recording of relative dot replacements with a 70-mm camera is satisfactory for strains greater than 2%. Photoelastic coatings could be used for the non-equal biaxial strain state at a sacrifice to reinforcement effects. Moire fringes could also be used for strains less than 5%. These methods will be evaluated and compared at a future date. Since the primary interest in this study program is solid propellant, strains greater than 50% will not be considered. Primary interest is in strain values up to 20%.

The change in thickness can be measured approximately by means of two linear resistance gages. In this manner thickness change versus resistance change can be recorded.

### 4. The Strain Energy Function

The concept of strain energy used in this study is more general than the time-independent potential function that has usually been exploited in the literature. Following Noll (Ref. 20), the idea of memory (i.e., a strain energy function being a function of time as well as geometry) is being considered for solid propellant. The generality of such a functional affords a great number of possibilities to the experimenter for characterization of data. A method was proposed to characterize an approximate strain energy function in QSR 38-11. This method

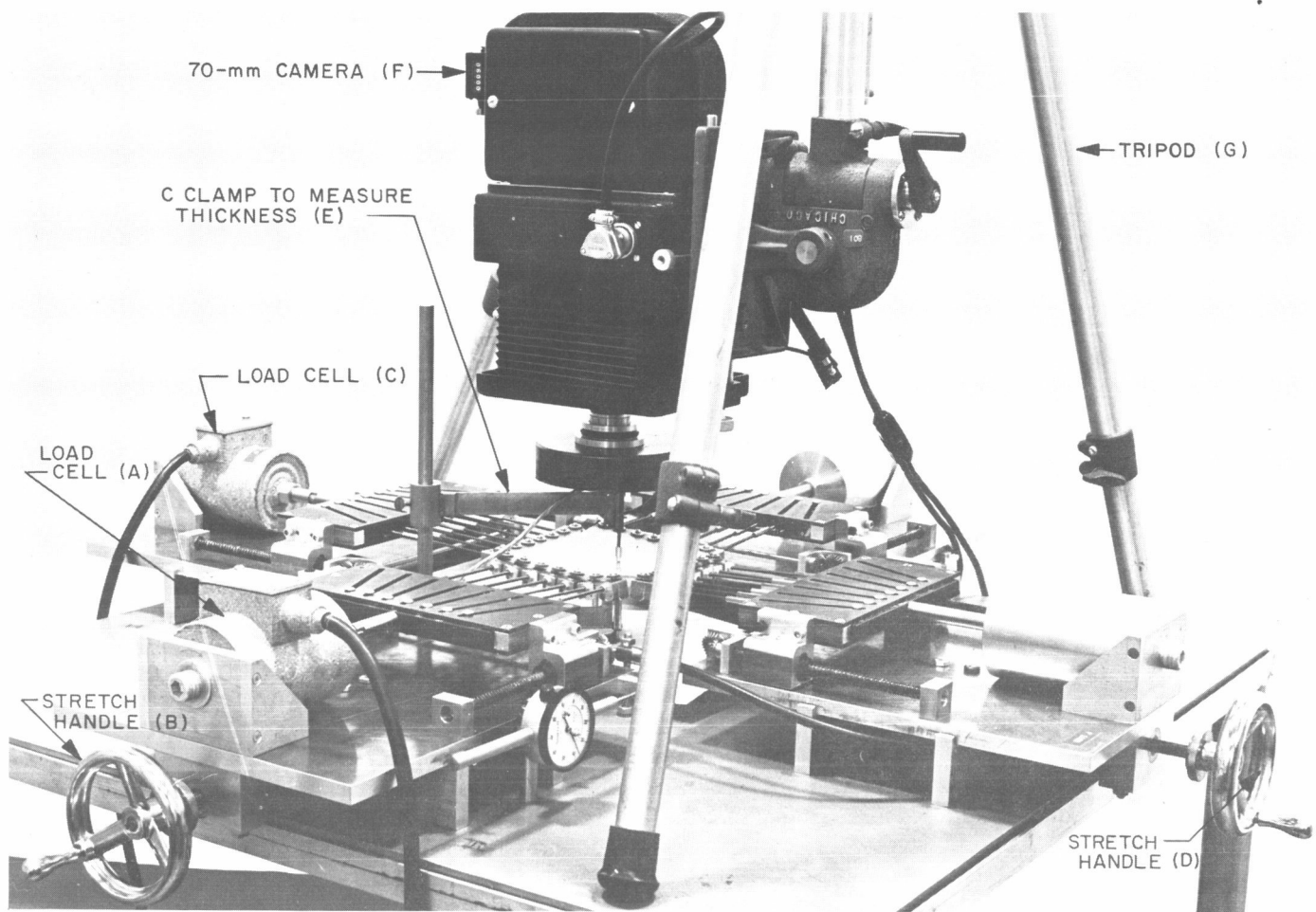


Fig. 23. First construction phase of the tension-tension biaxial tester

was examined, using stresses and strains obtained from the inflated cylinder test (QSR 38-10). It is suggested that the results obtained by this method should be comparable to any other multiaxial test if the method is indeed valid.

### 5. Apparatus

The first construction phase of the tension-tension biaxial stress tester is shown in Fig. 23. The apparatus consists basically of two load cells (A and C), two manual stretch handles (B and D), a C-clamp with resistance gages to estimate thickness changes (E), and a 70-mm camera (F) mounted on a sturdy tripod (G). Fig. 24 illustrates the functioning of the apparatus. As shown here, a 200-lb load cell has been inserted in the center so as to calibrate the individual load cells. This calibration was deemed necessary to show that a negligible amount of friction existed throughout the apparatus.

An extension in the 1-direction, independent of the 2-direction, is obtained by rotating the stretch handle C. This is accomplished by a screw action on both plates H and J. Simultaneously, the two flexible cables K and L activate screws M and N relative to plates O and P. Thus, a rotation of stretch handle C activates plates H and J equally and guides Q and R. Analogously, a rotation of stretch handle D activates plates O and P equally and guides S and T. Dial indicators U and V record relative displacement of plates H, J, O, and R relative to the base table W.

The mechanism of the guides can best be described by the illustration in Fig. 25. Upon rotation of the flexible cable K, the two guide screws X and X<sup>1</sup> are activated by the pinion gears Y and Y<sup>1</sup>. Guides Q (upper and lower) consequently move with respect to the bar Z. This bar Z is attached on one side to the load cell by means of a universal joint and on the other side to the biaxial sheet.

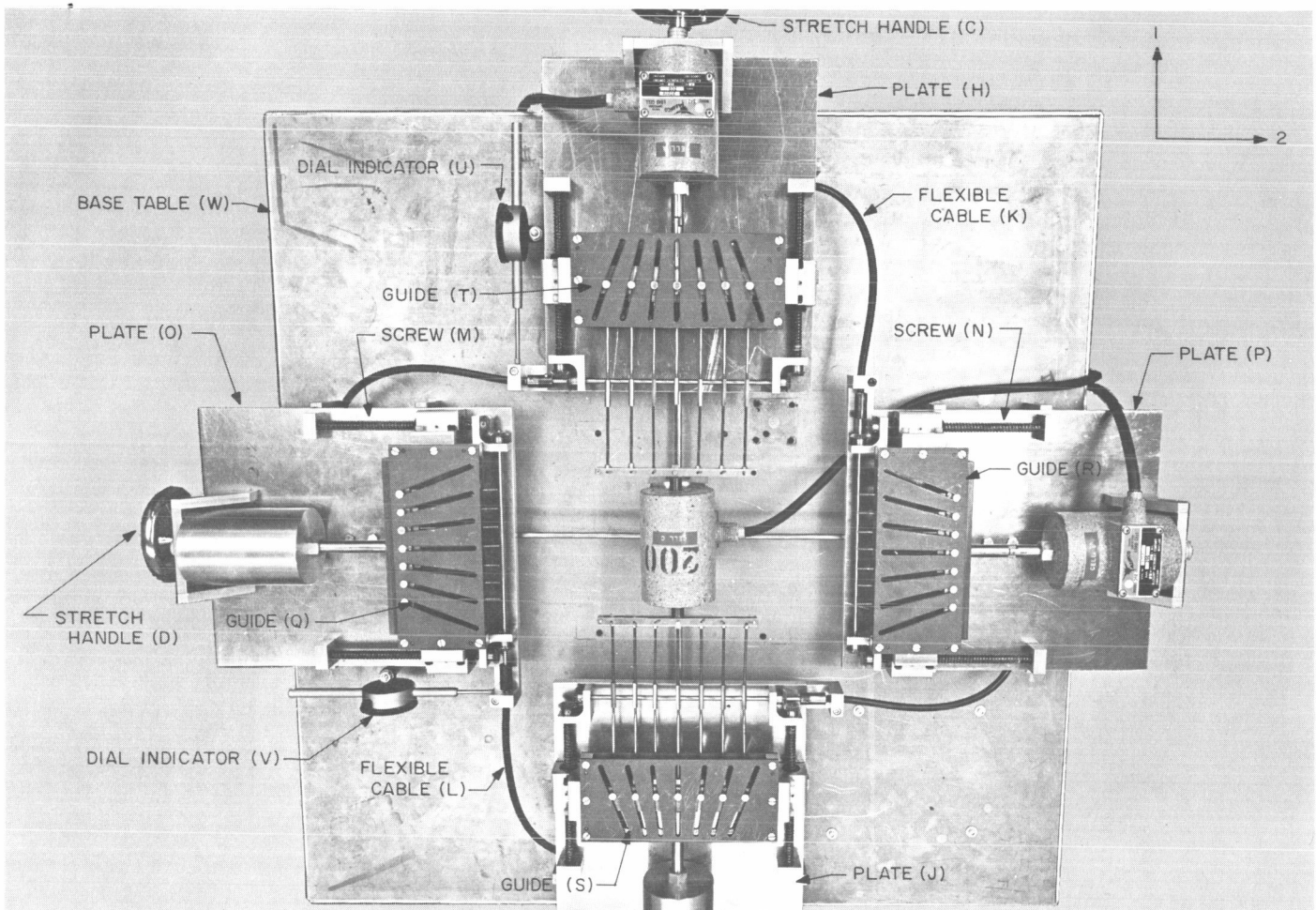


Fig. 24. Functional aspects of the biaxial tester

Seven pins transmit the load between the bar Z and the biaxial sheet. The pins are free to move along the bar Z. Hence, by sliding the identical upper and lower guide plates with respect to the bar Z, the pins must assume a unique position with respect to each other. Thus, the only action associated with a cross extension is the repositioning of the pins in bar Z.

The apparatus is essentially geometry-controlled, although it could be load-controlled by means of a suitable servomechanism. The angles of the slots in the guide plates are governed by the geometry of the biaxial test specimen. The arbitrarily selected geometry is shown in Fig. 26 for a sheet of propellant. This propellant sheet is 6 × 6 in. in the plan view and is 0.110 in. thick. A tensile specimen is also shown in the figure. This tensile specimen was used to obtain uniaxial data. Two fractured resin biaxial specimens (resin 283C and resin motor sheets) are shown in Fig. 27. The larger specimen (resin

283C) was fractured by equal biaxial strains ( $\epsilon_1/\epsilon_2 \approx 1$ ), the smaller specimen (resin motor) was fractured by unequal biaxial strains ( $\epsilon_1/\epsilon_2 \approx 2$ ). Specimen size was selected as a compromise between two undesirable effects. The sheet had to be small enough so that inertial effects would not contribute to a sag in the center. At the same time, it had to be large enough so that a uniform biaxial stress state could be imposed upon it. It was felt that the 6 × 6 in. geometry was a fair compromise for polyurethane propellant.

The clamping technique found to be most satisfactory is not shown in the figures but is a modification of the clamps shown. A satisfactory clamp consists of a U-shaped geometry with a fastened bolt and nut. The mating propellant or resin sample consists of a hole reinforced by two bonded flat washers. The sacrifice to local stress concentrations (readily observed in a photoelastic specimen) is more than repaid for by tear insurance at the

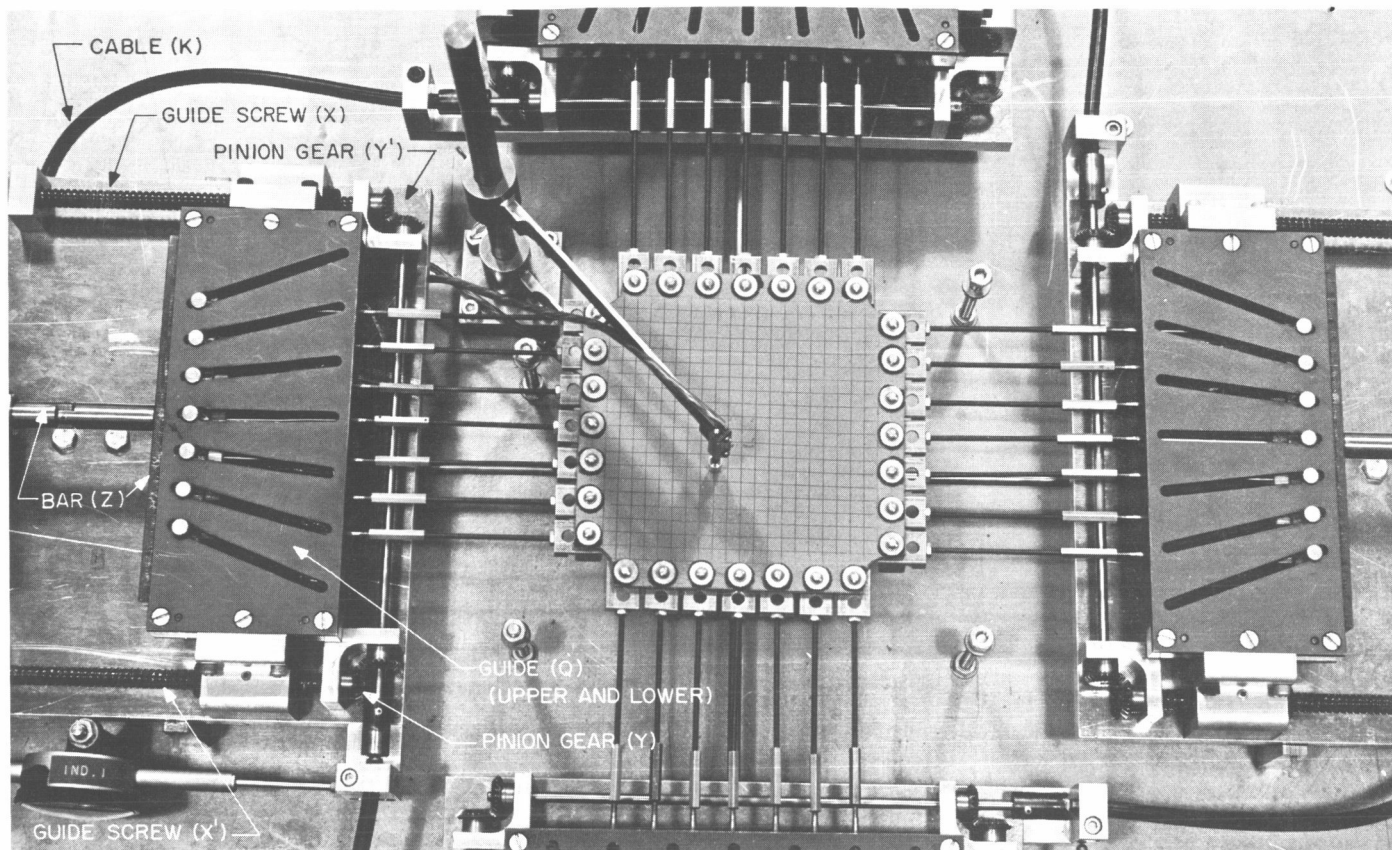


Fig. 25. Plan view of guide mechanism

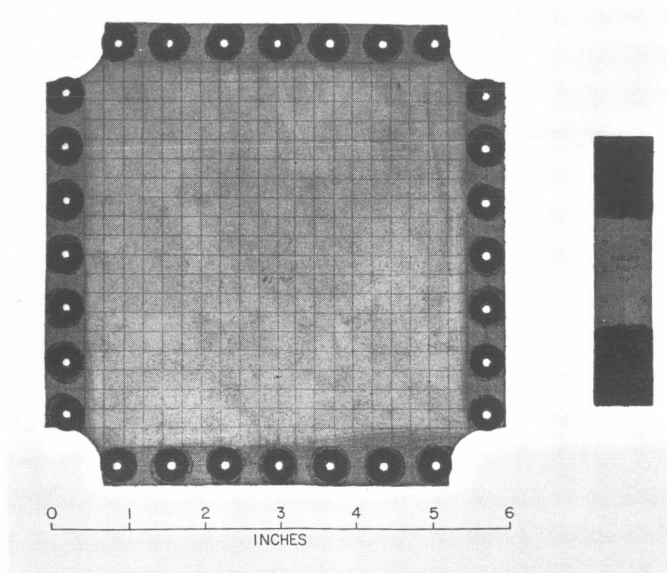


Fig. 26. Solid propellant biaxial sheet and tension strip

attachment. The tear of the specimens ( $\epsilon_1/\epsilon_2 \approx 1$  for the larger sheet,  $\epsilon_1/\epsilon_2 \approx 2$  for the smaller sheet) in Fig. 27 was initiated at the radius, *not* the attachment.

The second phase of improvement to this instrument will consist of additions of two variable speed motors to drive the manual stretch handles, development of a more accurate thickness measuring transducer, and an implementation of a data-recording system to make simultaneous readings with reference to the same time scale. With these improvements it will be possible, with a minimum of scatter, to get data for biaxial strain ratios ( $\epsilon_1/\epsilon_2$ ) under transient loading, creep, and relaxation. Photoelastic studies are also contemplated upon installation of a light bank beneath the specimen.

## 6. Discussion

A rational procedure to evaluate the biaxial tester is to examine a sheet of a rubberlike material (Solithane 113) experimentally. A rubberlike material was chosen

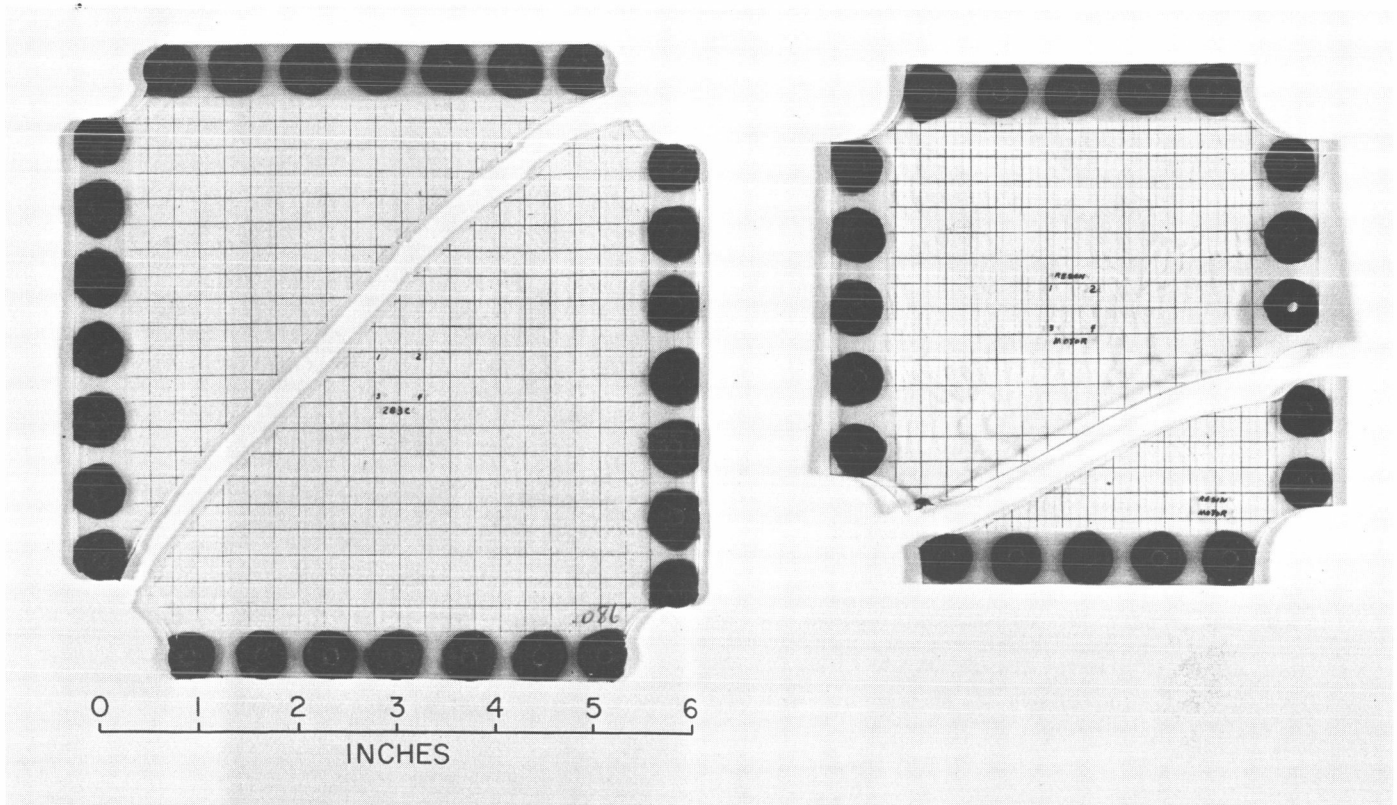


Fig. 27. Fractured resin 283C resin sheet ( $\epsilon_1/\epsilon_2 \approx 1$ ) and fractured resin motor sheet ( $\epsilon_1/\epsilon_2 \approx 2$ )

because it is relatively linear, homogeneous, isotropic, and elastic. Inference can then be made about the propellant stress-strain response with reference to this analogous simple material.

Fig. 28 records the biaxial strain states of resin 283C, which is an unfilled polyurethane sheet (the largest sheet in Fig. 27). Each point on the graph is uniquely determined by one of an infinite number of geometries (strain states) that can be imposed by the biaxial instrument. The point to be made is that it is difficult to hold the strain ratio ( $\epsilon_1/\epsilon_2$ ) constant with the existing manual stretch handles. This polyurethane sheet can reasonably be considered incompressible. Hence, the data of Fig. 28 can be used in conjunction with the incompressibility equation [Eq. (3)] to obtain the corresponding thickness strains  $\epsilon_3$ , as shown in Fig. 29. Strain measurement errors associated with  $\epsilon_1$  and  $\epsilon_2$  are not observed to be severe by this unusual error analysis. Because of the difficulty in maintaining the strain ratio  $\epsilon_1/\epsilon_2$  constant, only one run was performed ( $\epsilon_1/\epsilon_2 \approx 1$ ).

A second polyurethane resin was examined for two ratios,  $\epsilon_1/\epsilon_2 \approx 1$  and 2. This resin was cast from the same

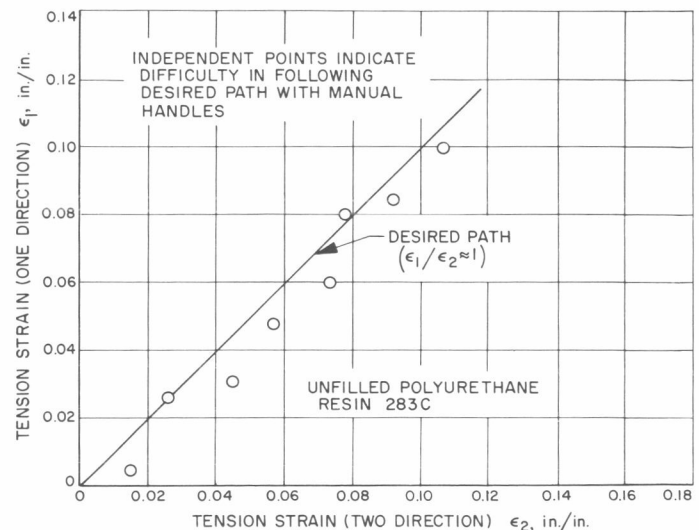
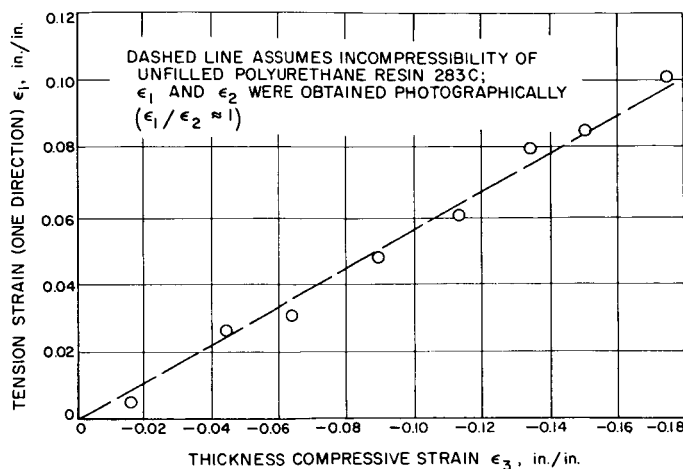


Fig. 28. Deviation between desired straining ratio ( $\epsilon_1/\epsilon_2 \approx 1$ ) and actual (resin 283C)

batch as the tensile bar and thick-walled cylinder reported in QSR 38-12. The smaller geometry (Fig. 27) resulted from the idea that the biaxial specimen should have tabs. Preliminary experiments revealed that tabs



**Fig. 29. Thickness strain assuming incompressibility (resin 283C)**

were undesirable for the low strain-fracture materials being studied in this program. Hence, trimming the tabs reduced the magnitude of the geometry. Figs. 30 and 31 are analogous to Figs. 28 and 29 in all respects. Figs. 32 and 33 are also analogous to Figs. 28 and 29 except that  $\epsilon_1/\epsilon_2 \approx 2$ .

Two dummy polyurethane propellant (Fig. 26) sheets were next subjected to straining at ratios of  $\epsilon_1/\epsilon_2 \approx 1$  and 2, respectively. Figs. 34, 35, 36, and 37 are interpreted in the same manner as Figs. 30, 31, 32, and 33 for the unfilled polyurethane sheet. This analogy can be inferred because no mention of stresses or physical prop-

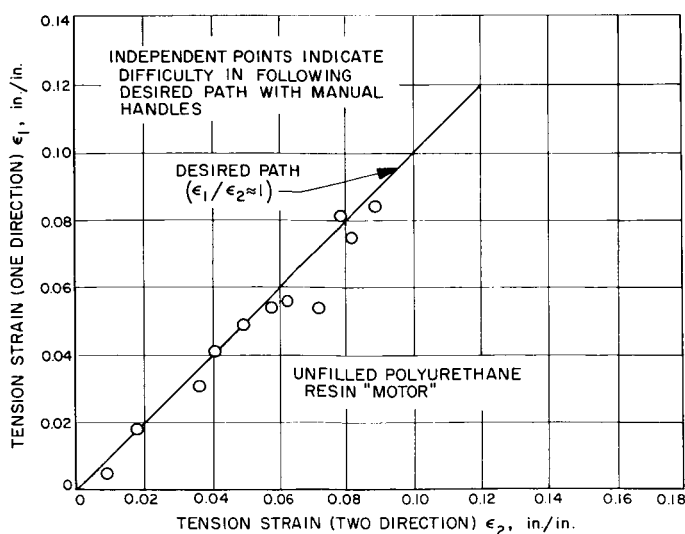


**Fig. 30. Deviation between desired straining ratio ( $\epsilon_1/\epsilon_2 \approx 1$ ) and actual (resin motor)**

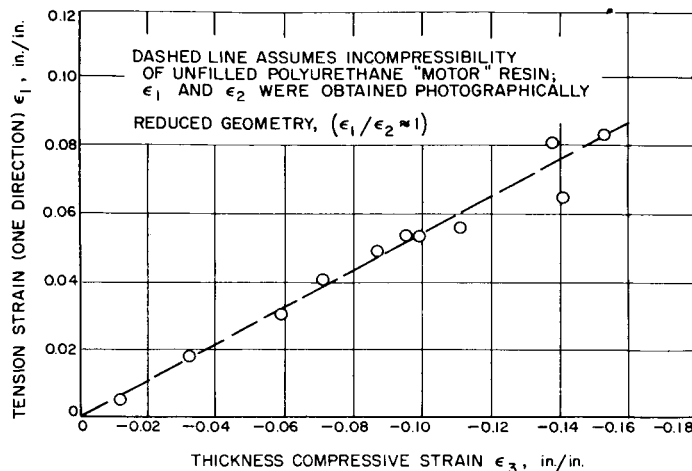


**Fig. 31. Thickness strain assuming incompressibility (resin motor)**

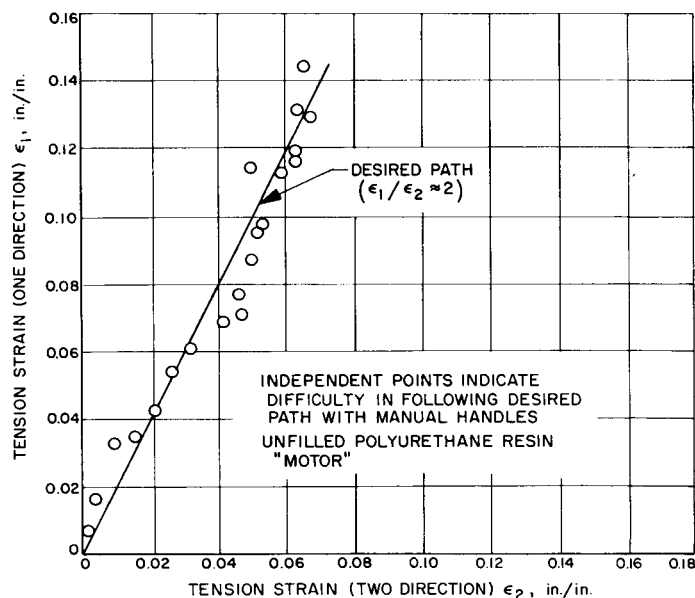


**Fig. 32. Deviation between desired straining ratio ( $\epsilon_1/\epsilon_2 \approx 2$ ) and actual (resin motor)**

erties has yet entered this discussion. The critical observation here is that the slope of the measured  $\epsilon_1$  versus  $\epsilon_3$  for the propellant is approximately that computed, assuming incompressibility, from the experimental unfilled polyurethane biaxial strains. This is shown by comparison of Fig. 35 to Figs. 29 or 31, and Fig. 37 to Fig. 33. These data were obtained for both the loading and unloading parts of the loading cycle. Experimental difficulties in measuring all the parameters in a short period of time were experienced because of the dewetting phenomenon. Hence, some out-of-phase recording of various parameters was inevitable. This situation will be eliminated in

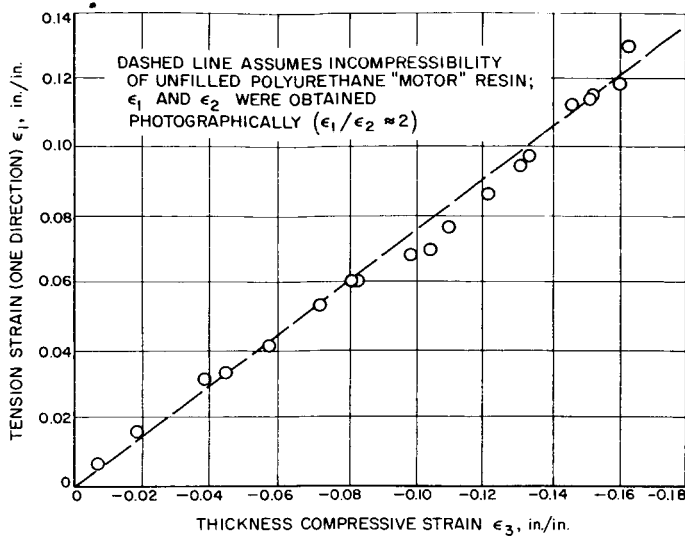


**Fig. 33. Thickness strain assuming incompressibility (resin motor)**

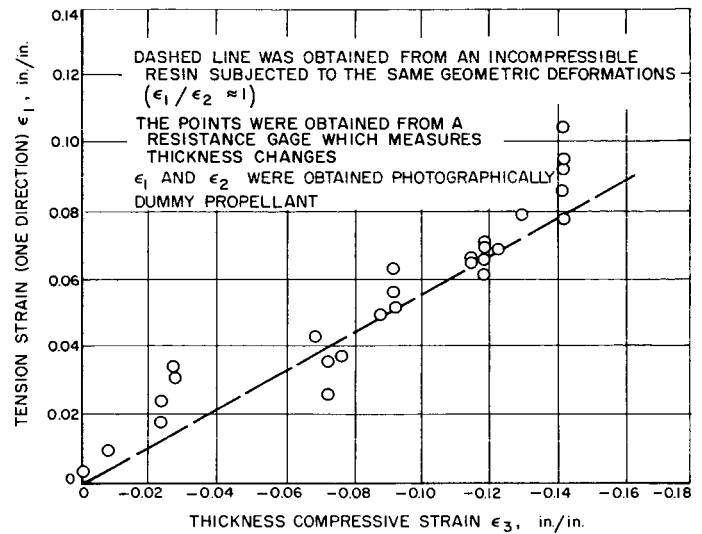


**Fig. 35. Measured thickness strain compared to incompressible assumption strain (dummy propellant)**

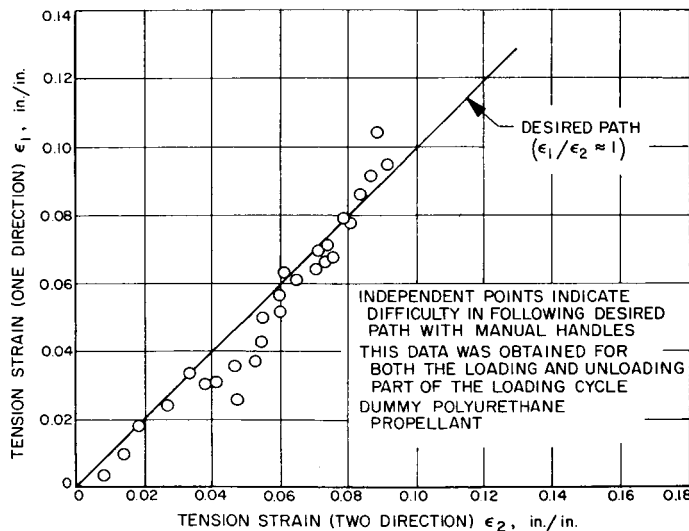


**Fig. 34. Deviation between desired straining ratio ( $\epsilon_1/\epsilon_2 \approx 1$ ) and actual (dummy propellant)**

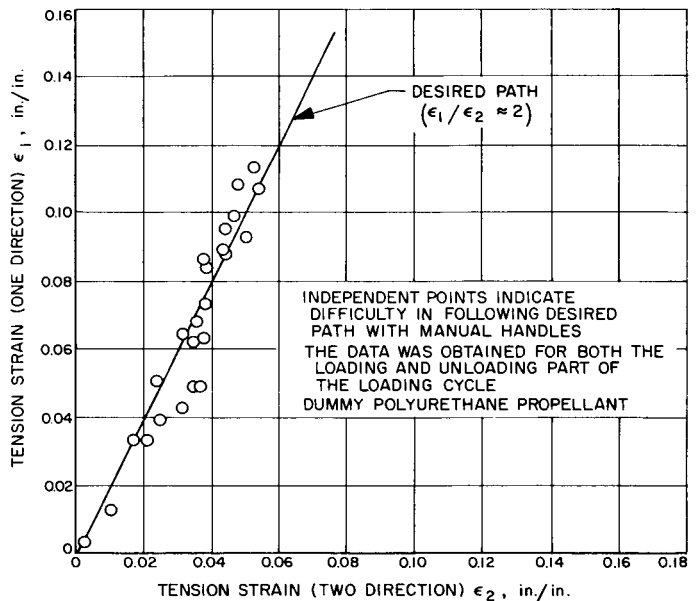


**Fig. 36. Deviation between desired straining ratio ( $\epsilon_1/\epsilon_2 \approx 2$ ) and actual (dummy propellant)**

the future. The experimentally obtained thickness change, measured with a simple resistance transducer, should be improved (Figs. 35 and 37). On the other hand, a line drawn through the data gives an approximate "measured" strain value for theoretical computations. However, in the theoretical computations to follow, the actual scatter data was used in order to observe the maximum possible deviations in the strain energy magnitudes.

The values of Poisson's ratio  $\mu$  and Young's modulus  $E$  were measured for the unfilled polyurethane resins by

means of a uniaxial tensile test. With these values and the biaxial strains  $\epsilon_1$  and  $\epsilon_2$ , the biaxial stresses at the center of the rubber sheet were computed using Eq. (2). This information, together with the load cell measurements, at the boundaries of the sheet, enables the computations of effective lengths,  $L_1$  and  $L_2$ , defined from the

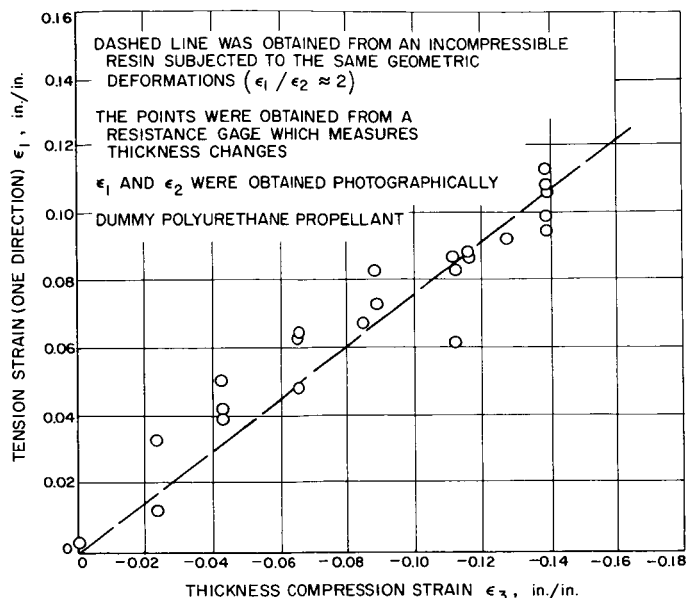


**Fig. 37. Measured thickness strain compared to incompressible assumption strain (dummy propellant)**

pseudostresses of Eq. (5), using the reasonable assumption of Eq. (6). Fig. 38 is the experimentally observed relationship between biaxial strain at the center of the sheet and effective length of the entire sheet. If the deformed geometry of the rubber sheet (e.g., 10% strain) approximates the deformed geometry of the propellant sheet (e.g., 10%) then the relationships shown in Fig. 38 should be applicable to the propellant sheet because of equilibrium considerations, e.g., this is analogous to the concept of the Airy stress function, which is independent of the material properties.

The data scatter in Fig. 38 is due in part to the following reasons: (1) the strain ratios  $\epsilon_1/\epsilon_2$  could not be maintained constant for any continuous experimental run; (2) the resin "motor" sheet (Fig. 27) dimensions were less than those for which the biaxial tester was designed; (3) the data input was obtained using a number of different instruments to make measurements (a multichannel recorder which has a time reference base should be used instead of having three operators manipulating handles and reading dials) and (4) ordinary experimental error. Hence, the scatter precludes accurate empirical curve fitting. On the other hand, this first phase of checkout of the biaxial tester was not expected to produce accurate data. It was intended to be a rough check to establish where improvements were really needed. For example, it appears that a family of curves can be

generated for different constant strain ratios  $\epsilon_1/\epsilon_2 = 1, 2 \dots n$ . This family of curves may diverge from the reference curve  $\epsilon_1/\epsilon_2 = 1$ . In any event, the scatter is not intolerable for resin 283C, which had the proper geometric dimensions for which the instrument was designed. These dimensions are the same as those for the dummy propellant sheet (Fig. 26). Hence, these curves can be used as an approximation to the effective lengths of the dummy propellant sheets.

Using the values of effective length obtained from Fig. 38 for any given propellant strains, the true stresses in the center of the propellant can be computed from Eq. (5). These multiaxial stresses and strains are graphed in Figs. 39a and b, and 40a and b for  $\epsilon_1/\epsilon_2 \approx 1$  and  $\epsilon_1/\epsilon_2 \approx 2$ , respectively. A linear relationship is observed in all the four graphs. The data scatter is not severe, considering all the inputs discussed above. One might speculate that significant creep was initiating at 8% strain for the  $\epsilon_1/\epsilon_2 \approx 1$  condition (Figs. 39a and b). In any event, once the test is perfected, creep and relaxation responses should be readily detected to gain further insight into the applicability of the proposed theory to propellant stress-strain response.

Recall that the effective lengths for the unfilled polyurethane resins were computed assuming that the stresses at the center of the sheet could be set equal to homogeneous pseudostresses for the entire sheet. The stresses at the center of the sheet,  $\tau_1$  and  $\tau_2$ , were computed from the classical theory of elasticity given the measured biaxial strains and material constants, obtained from a tensile test. Now, if the polyurethane resin is indeed classically elastic, a straight line relationship between experimentally obtained strain and experimentally obtained stresses (using experimentally obtained effective lengths) should be observed. Figs. 41a and b, 42a and b, and 43a and b demonstrate that this linear relationship does indeed exist for resin 283C and the resin motor where  $\epsilon_1/\epsilon_2 \approx 1$ , and for the resin motor where  $\epsilon_1/\epsilon_2 \approx 2$ , respectively. Note that each experimentally obtained point was obtained in an independent manner. For these points to fall in a straight line implies that the material is linear, homogeneous, isotropic, and elastic. The slope of  $\epsilon_1$  versus  $\tau_1$  is the same as the slope of  $\epsilon_2$  versus  $\tau_2$  for the condition of  $\epsilon_1/\epsilon_2 \approx 2$  as would now be expected.

The experimental scatter is considerably better for the resin than that for the propellant. It is suspected in light of this evidence that perhaps creep and relaxation are being experienced by the propellant, and hence the time

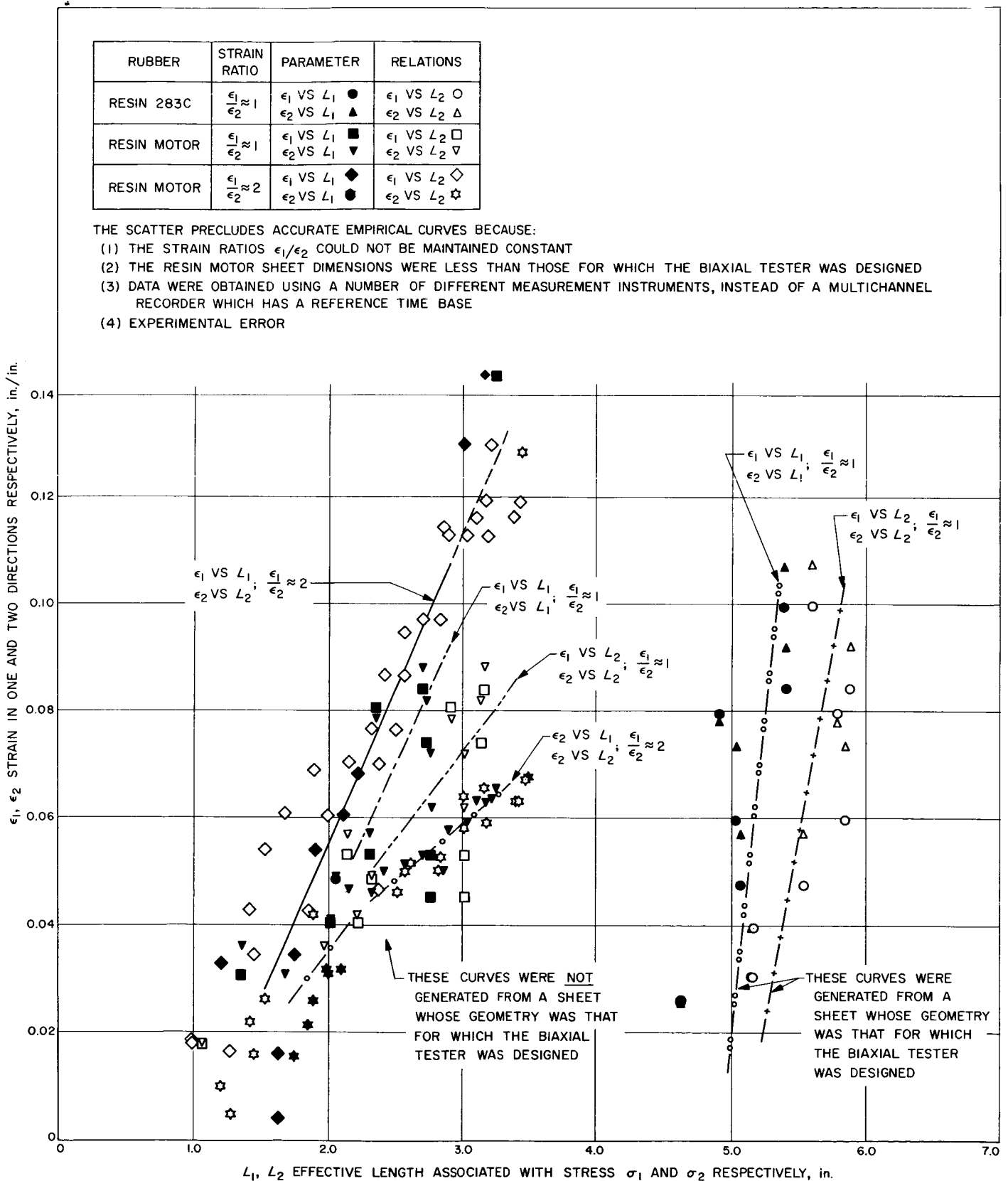


Fig. 38. Measured strain versus effective lengths for resin sheets

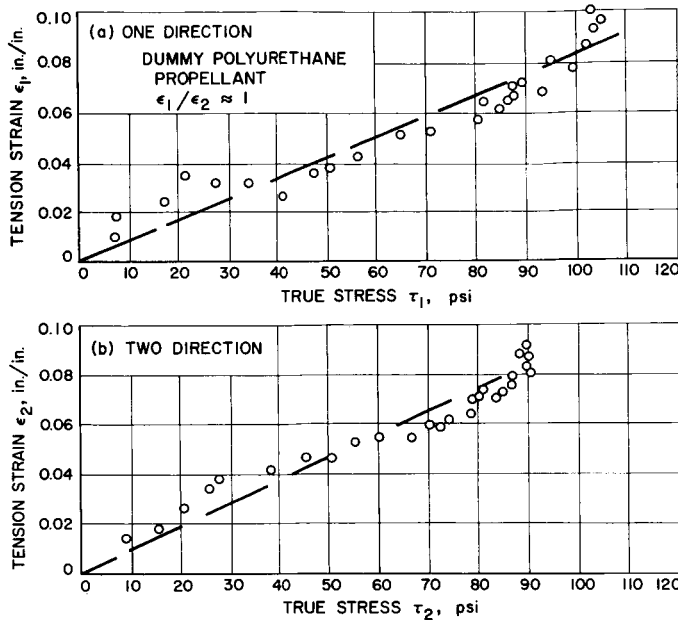


Fig. 39. Strain vs stress,  $\epsilon_1/\epsilon_2 \approx 1$ , dummy propellant, (a) longitudinal, (b) transverse

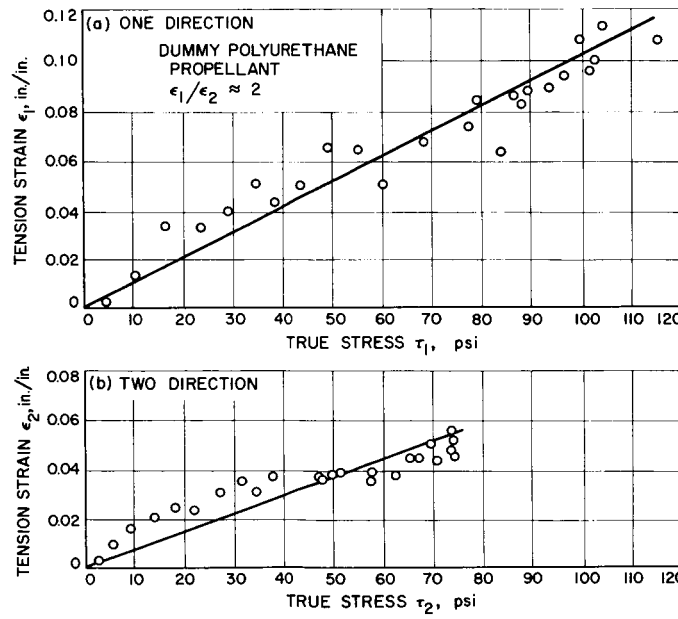


Fig. 40. Strain vs stress,  $\epsilon_1/\epsilon_2 \approx 2$ , dummy propellant, (a) longitudinal, (b) transverse

base of the data obtained in a crude manner for the propellant was out of phase. This would cause greater scatter in the propellant data than would be contributed by the instrumentation. A comparison of the slope of  $\epsilon_1$  versus  $\tau_1$  for the propellant (Figs. 39a and b) with resin 283C (Figs. 41a and b) and with the resin motor (Figs.

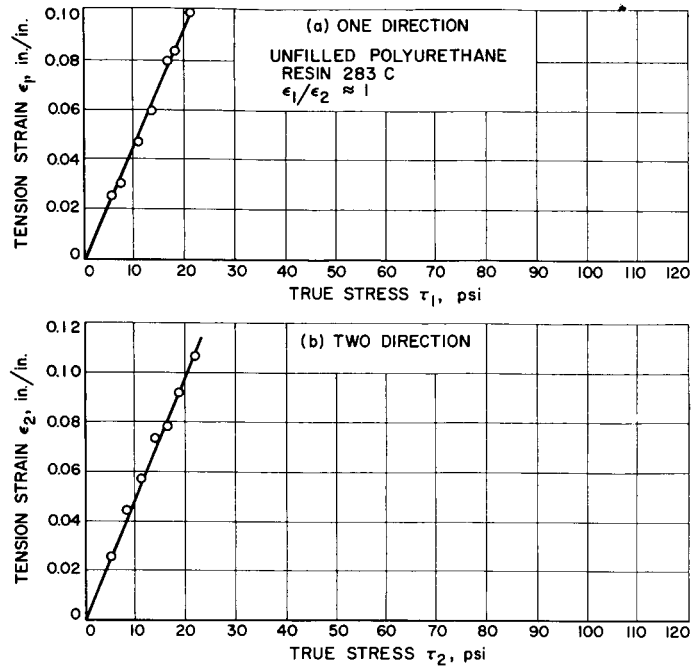


Fig. 41. Strain vs stress,  $\epsilon_1/\epsilon_2 \approx 1$ , resin 283C, (a) longitudinal, (b) transverse

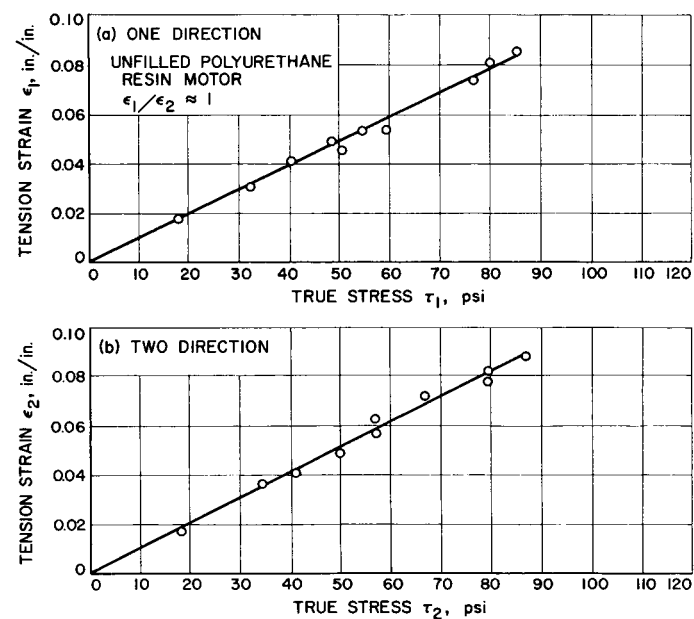


Fig. 42. Strain vs stress,  $\epsilon_1/\epsilon_2 \approx 1$ , resin motor, (a) longitudinal, (b) transverse

42a and b) indicates that the modulus of the propellant should be slightly higher than the resin motor and significantly higher than resin 283C. The same observation holds by inspection for Figs. 40a and b and Figs. 43a and b.

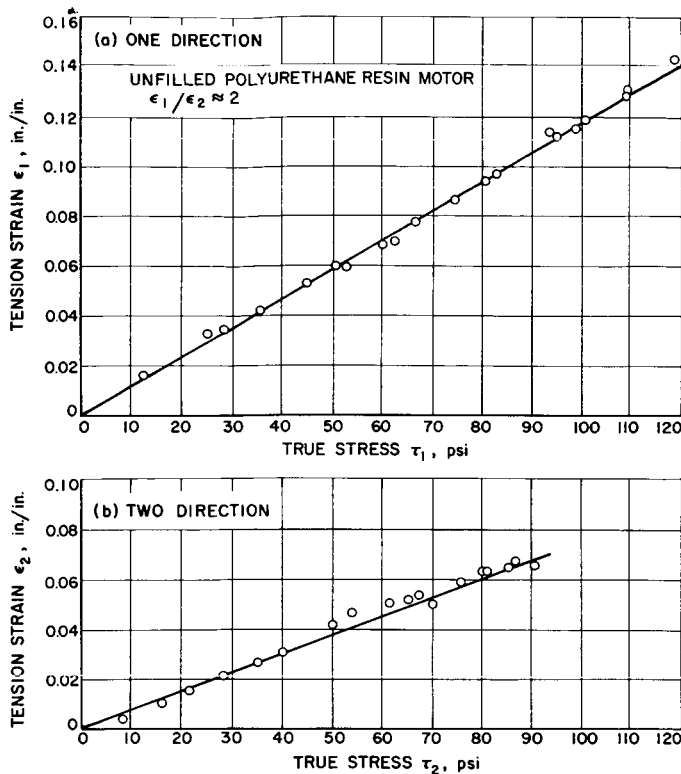


Fig. 43. Strain vs stress,  $\epsilon_1/\epsilon_2 \approx 2$ , resin motor, (a) longitudinal, (b) transverse

Tensile data for the unfilled resins, 283C and the resin motor, together with the dummy polyurethane propellant are shown in Figs. 44a and b. This tensile data confirms the above observations regarding moduli. Dewetting of the dummy propellant is evident for strains greater than 5%. The propellant is nonlinear for greater strains. An interesting observation is that the stress-strain data of the propellant are irregular compared to the resin data (both were obtained in an identical manner).

This same observation was made in the biaxial data (Figs. 40a, b, and 41a, b). Another interesting observation is that the propellant biaxial stresses reached a higher magnitude (100 psi) than the uniaxial test indicated was possible (90 psi). These high stress values were obtained at a substantially smaller strain state (+8%, +8% versus +45%, -14%). This same observation, that the stress state is larger for a smaller strain state, agrees with the unfilled polyurethane data. However, it is not obvious why the stress state at the center of the biaxial sheet can be greater than the maximum stress obtained from a tensile test.

Although the tension-tension biaxial stress-strain data have a great deal of scatter (this will be improved upon in the near future), it would be interesting to see and to compare values of strain energy and strain energy partial derivatives versus strain invariants obtained from the sheet test, with those obtained previously (QSR 38-12) for the inflated cylinder test (QSR 38-10). The inflated cylinder data found in QSR 38-10, Figs. 16, 17, are for an ammonium perchlorate polyurethane propellant, whereas the data found in QSR 38-12, Table 8, p. 33, are for the resin motor (unfilled Solithane 113). Thus, if similar results can be obtained from this tension-tension biaxial experiment, then the inflated cylinder test in conjunction with the proposed theory will be shown to be a powerful tool in the study of solid propellant mechanical properties.

Rivlin (Ref. 13) took great pains to measure for an incompressible rubber sheet the first strain invariant  $I_1$ , holding the second strain invariant  $I_2$ , constant. He then repeated his experiments (the third strain invariant  $I_3$ , was approximately one) measuring  $I_2$ , holding  $I_1$  constant. His measurements were for strain levels greater than 50% and as high as several hundred percent. Rivlin inferred from his results that  $\partial W/\partial I_1$  and  $\partial W/\partial I_2$  were

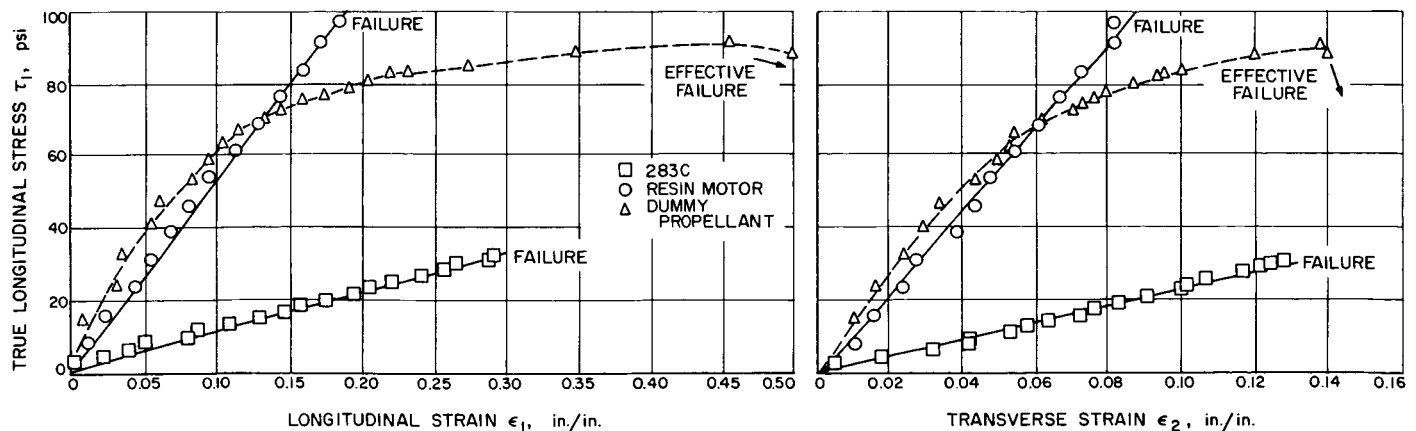


Fig. 44. Uniaxial stress vs strain

effectively independent of  $I_1$  and that  $\partial W/\partial I_1$  was effectively independent of  $I_2$ . However,  $\partial W/\partial I_2$  was not necessarily independent of  $I_2$ . These observations led to a possible form of the strain energy function for rubber as being

$$W = C_1 (I_1 - 3) + f(I_2 - 3) \quad (7)$$

Here  $C_1$  is constant, and  $f$  is a function of  $I_2$ . This possible functional form of  $W$  was chosen by assuming that the leading terms of a power series were sufficiently descriptive for rubbers.

It is recognized that the preceding work may be applicable for rubbers but not propellants. On the other

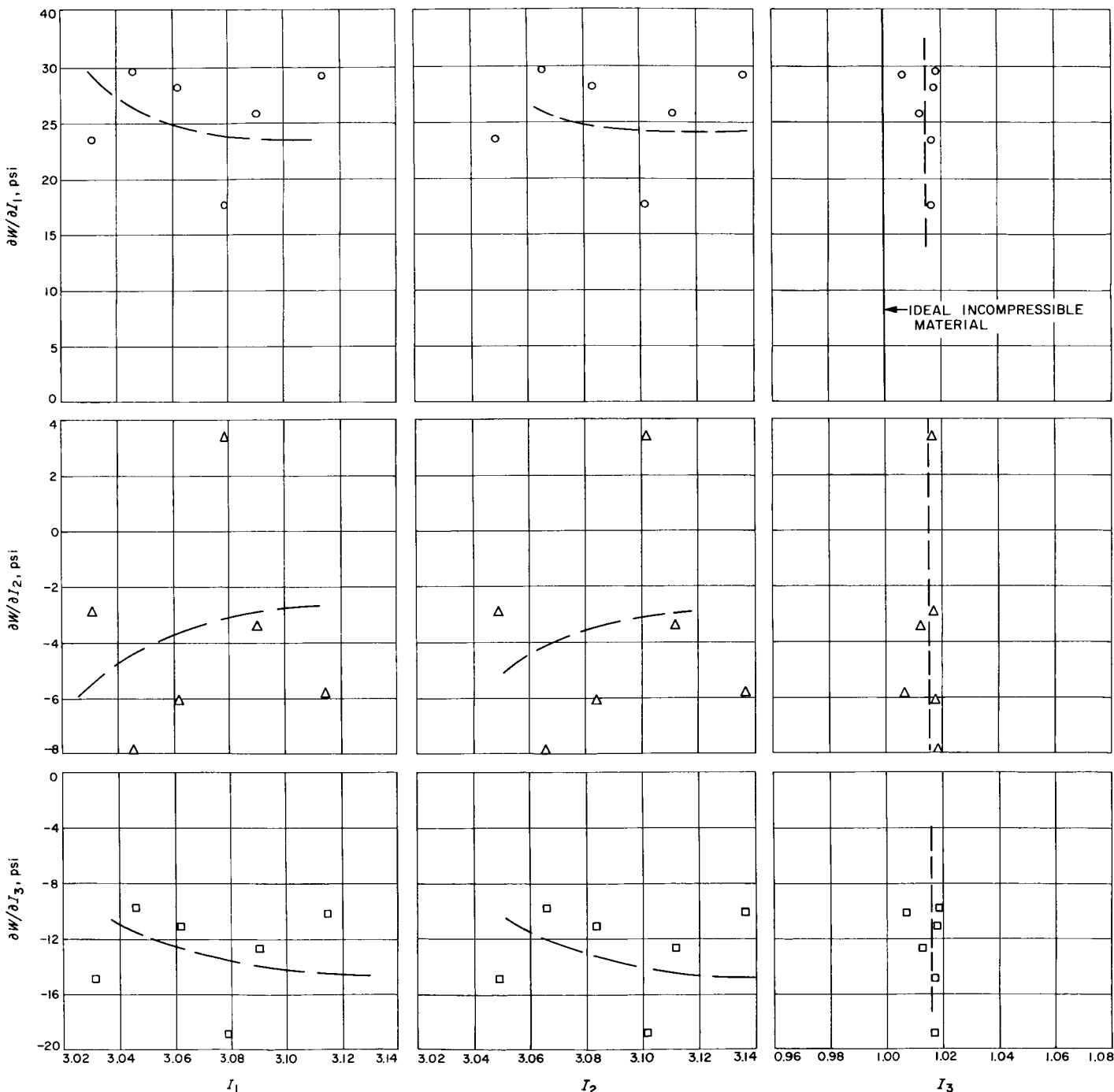


Fig. 45. Potential gradients versus the three invariants (resin 283C "sheet"  $\epsilon_1/\epsilon_2 \approx 1$ )

hand, the more general theory and experimentation necessary for solid propellant studies must at least degenerate into solutions for rubber materials if they are indeed to have any validity. It should be recognized that this study program is directed toward nonlinear viscoelastic phenomena. Hence, any interest in a strain energy function must include memory effects (QSR 38-13). This memory strain energy function must degenerate into the classical strain energy function of Rivlin, et al., for such materials as rubbers, or for that environment where solid propellant is essentially an elastic material in the classical sense.

Using the theory presented in QSR 38-10, the relationships between all the pertinent partial derivatives and strain invariants are shown in Fig. 45 for resin 283C. Aside from the undesirable scatter, the modes are quite indeterminate.

Definite modes are experienced for the partial derivatives and strain invariants of the resin motor sheet ( $\epsilon_1/\epsilon_2 \approx 1$ ) as illustrated in Fig. 46. For some reason (perhaps insufficient experience in running the experiment) the experimental data did not scatter as it did for resin 283C. Fig. 47 presents another set of data for the

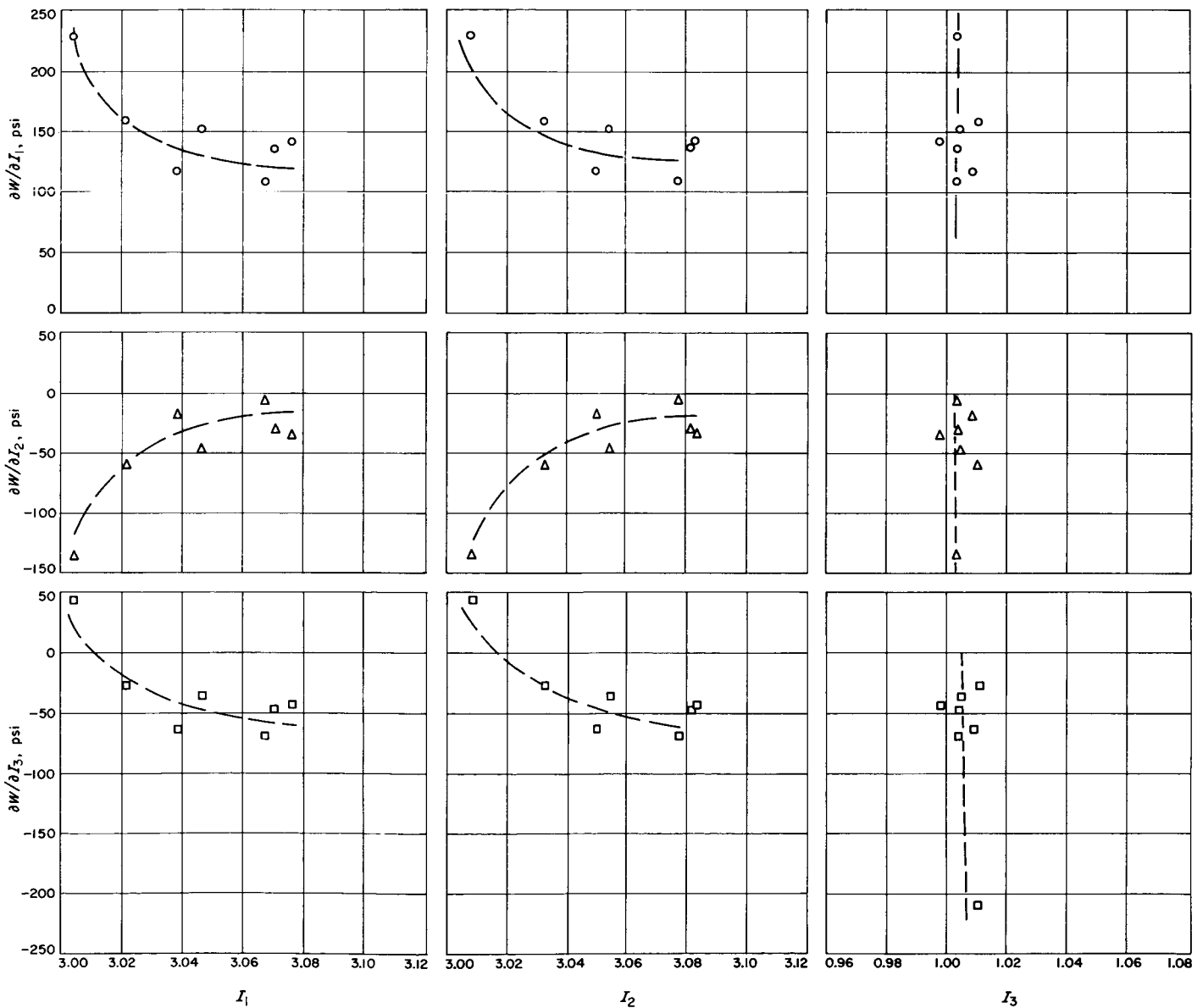


Fig. 46. Potential gradients versus the three invariants (resin motor "sheet"  $\epsilon_1/\epsilon_2 \approx 1$ )

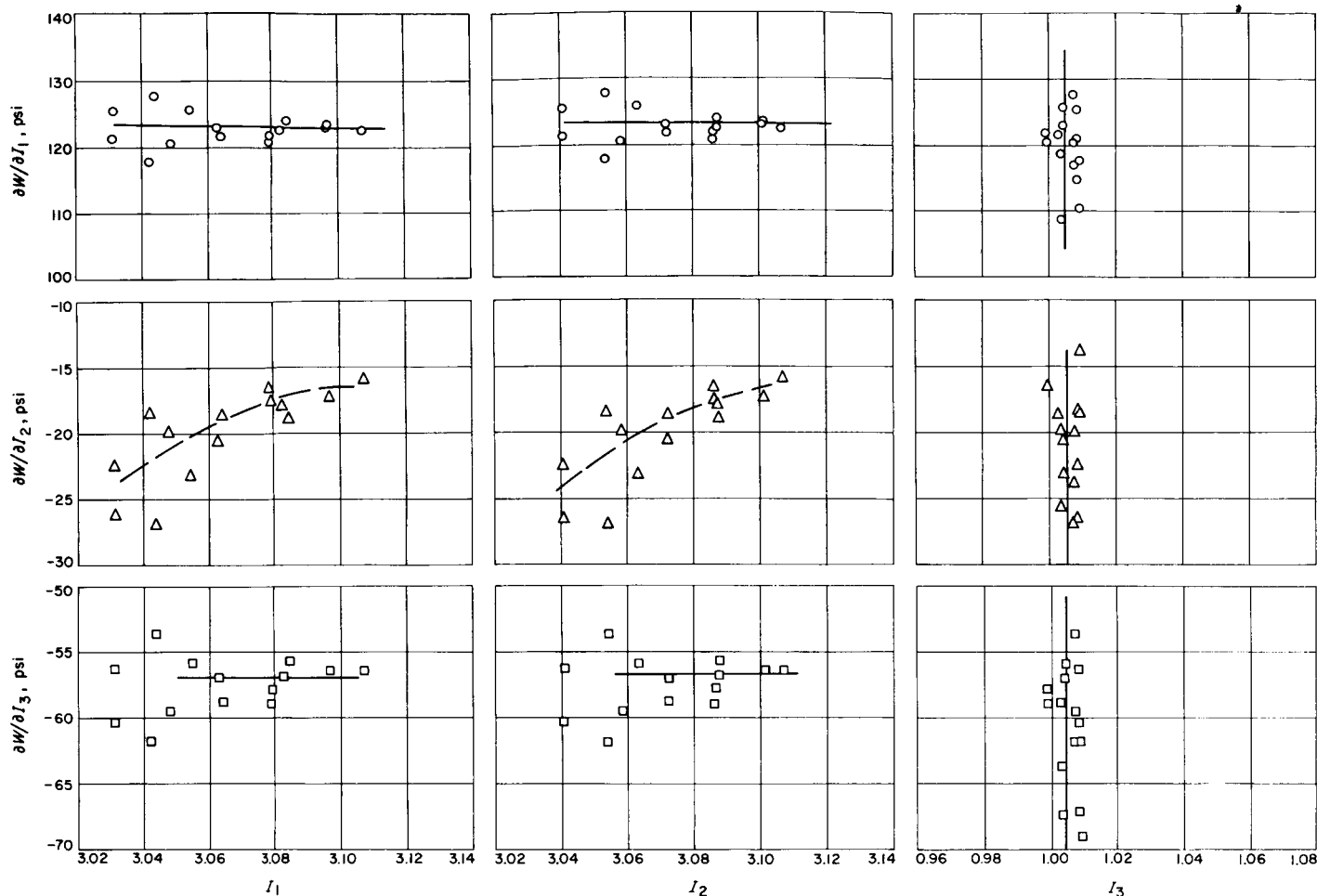


Fig. 47. Potential gradients versus the three invariants (resin motor "sheet"  $\epsilon_1/\epsilon_2 \approx 2$ )

same resin motor sheet ( $\epsilon_1/\epsilon_2 \approx 2$ ). These data substantiate both the mode and magnitudes of the parameters in Fig. 46. This is encouraging since a different loading field was being experienced for this test. One would expect such a unique set of curves if indeed a strain energy function is to have any merit for stress analysis.

Figs. 46 and 47 illustrate the advantages of pursuing a strain energy function for solid propellant stress analysis and mechanical properties studies. The ability to stress a material in any fashion and identify the strain state from a unique set of curves is a powerful asset. To test this hypothesis, it would be desirable to observe the relationships between the pertinent partial derivatives and strain invariants from an inflated cylinder test for a resin motor made of the same material as the sheet. Note that the stress-strain field for an inflated motor is quite different from that of a biaxial stretched sheet. This has been done (QSR 38-12) and the pertinent variables are plotted in Fig. 48. All the curves are vertical and asymptotic to

the ordinate. At first it would appear that no information was afforded by the inflated cylinder test. To the contrary, these curves superimpose quite well upon their counterparts in Fig. 46. Note that the intersecting magnitudes are about the same, even though a modest amount of aging occurred in the period between testing (six months in a desiccator). Hence, the inflated cylinder test served to fill in a portion of the sought-after curves. Another observation for the particular elastomers investigated is that  $\partial W/\partial I_3$  must be taken into account in any theory exploiting the strain energy concept, even though  $I_3 \approx 1$ .

Having established the validity (although a considerable amount of experimental scatter tended to obscure the results) of the proposed theory and the applicability of the two types of multiaxial tests with elastomers, attention is now turned toward the dummy propellant. Fig. 48 illustrates point locations of the partial derivatives and strain invariants analogous to those shown in Figs. 45,

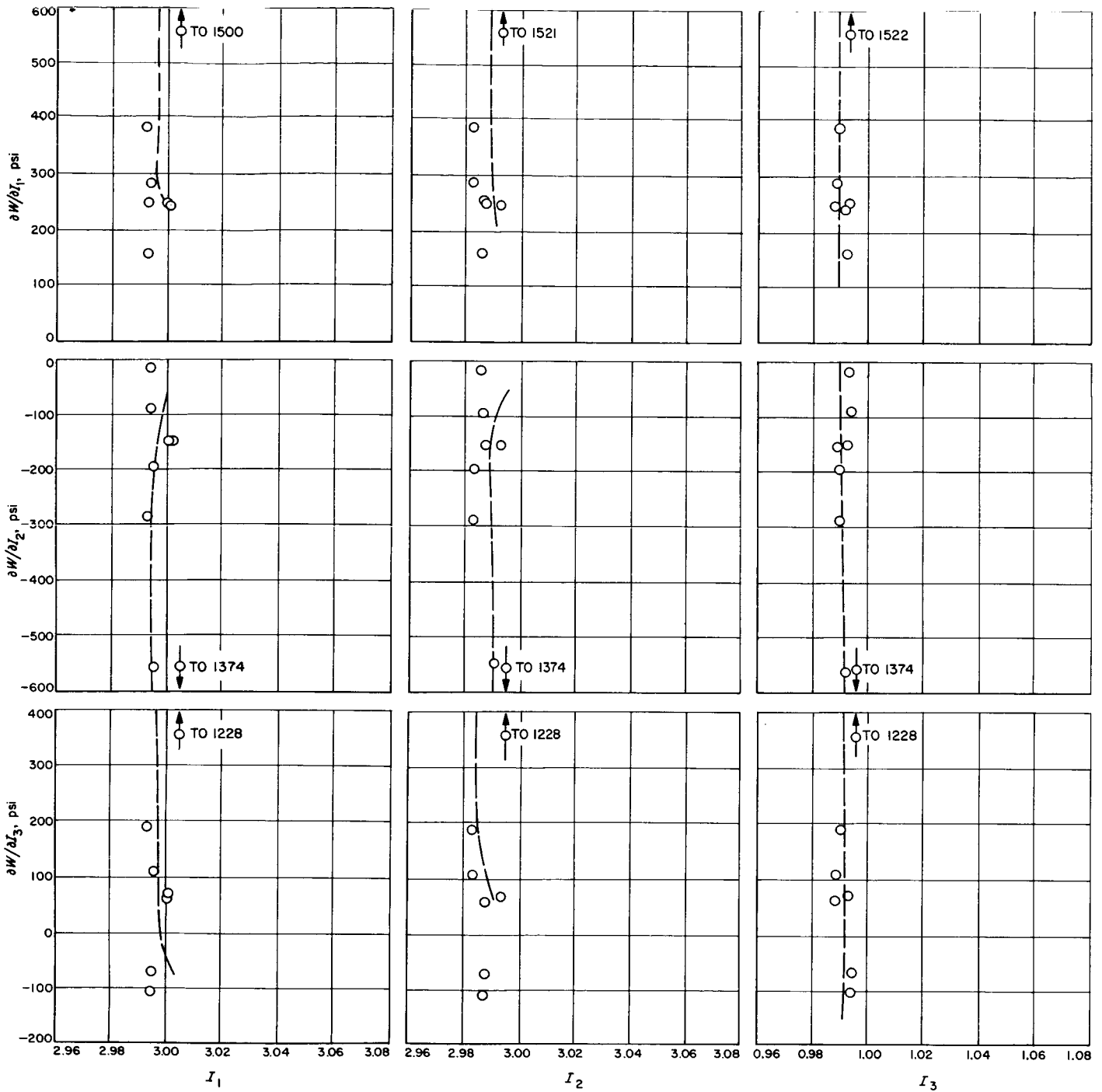
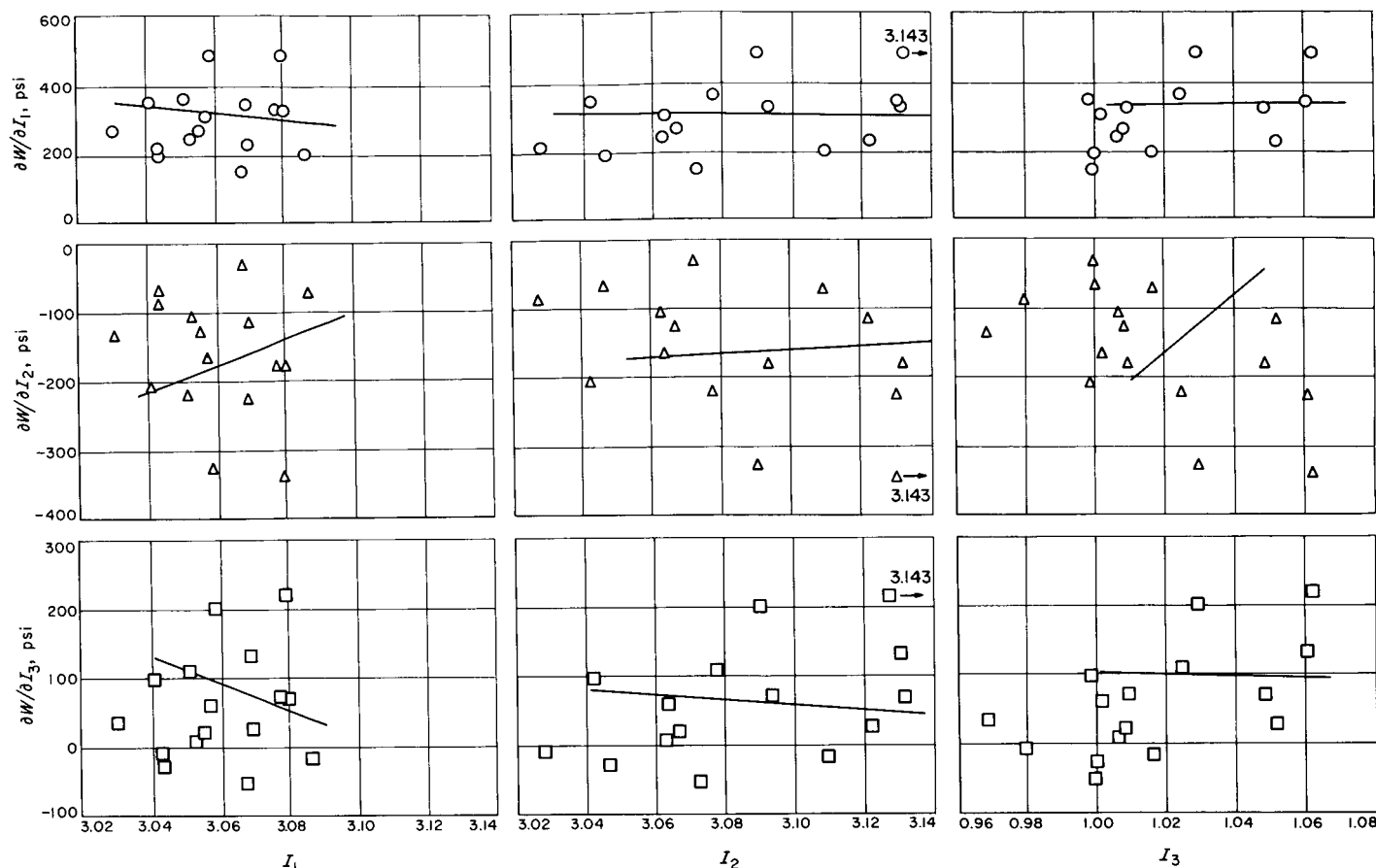


Fig. 48. Potential gradients versus the three invariants (resin motor "cylinder")

46, 47, and 48. The experimental scatter precludes any mode observations. Lines have been drawn in to speculate upon possible curve slopes. These directions are based on the modes assumed by the unfilled elastomers. Rationality dictates that some similarity should be expected between an unfilled elastomer and a filled elastomer experiencing small strains. By making the same

comparison between the data obtained from the inflated cylinder with that of the biaxial sheet, further insight may be gained as to the curve mode and magnitudes. In QSR 38-10, curves are shown for a polyurethane propellant whose properties are similar to those of the dummy polyurethane propellant. The superposition of Fig. 49 upon Fig. 16 in QSR 38-10 reveals as good a matching



**Fig. 49. Potential gradients versus the three invariants (dummy propellant  $\epsilon_1/\epsilon_2 \approx 2$ )**

(in mode and magnitude) as was observed above between Figs. 48 and 46. Although there is extreme scatter with the biaxial sheet data, it can again be surmised that the proposed theory and experimentation can be used to great advantage for solid propellant physical properties studies. Confirmation is again given to the fact that  $I_3$ , as well as  $\partial W/\partial I_3$ , must be included in any general theory of solid propellants.

The final observations to be taken into consideration concern the magnitude of the strain energy function as a function of the invariants. It is again proposed that strain energy (QSR 38-10) be defined as

$$W = \mathcal{U}(I_1 - 3) + \mathcal{V}(I_2 - 3) + \mathcal{H}(I_3 - 1)$$

It may now be stated the functional forms  $\mathcal{U}$ ,  $\mathcal{V}$ , and  $\mathcal{H}$  are functions of the invariants, or perhaps their derivatives. They are not the leading partial derivatives of the three dimensional Taylor's expansion, as had previously

been implied. A review of what is proposed as an initial theory is as follows:

- (1) It is proposed that the *magnitude* of strain energy  $W_i$  for any particular stress-strain state (eventually time will be included) can be approximated by the leading partial derivatives of a three-dimensional Taylor's expansion about a given  $I_1$ ,  $I_2$ , and  $I_3$  or

$$W_i = \frac{\partial W}{\partial I_1} (I_1 - 3) + \frac{\partial W}{\partial I_2} (I_2 - 3) + \frac{\partial W}{\partial I_3} (I_3 - 1)$$

where

$W_i$  is associated with an invariant set  $(I_1^i, I_2^i, I_3^i)$

- (2) By experimentally obtaining  $\partial W/\partial I_1$ ,  $\partial W/\partial I_2$ ,  $\partial W/\partial I_3$ ,  $I_1$ ,  $I_2$ , and  $I_3$  in some fashion (QSR 38-10)

so as not to have to assume anything about the material being characterized for a number  $i$  of equilibrium states, a number of independent magnitudes of  $W_i$  can be obtained.

- (3) If an empirical curve, unique only to the material being characterized, can be established for any loading condition (e.g.,  $W$  versus  $I_1, I_2, I_3$ ); then the strain energy concept would be established.

- (4) This empirical curve can be fitted by

$$W = \mathcal{H}(I_1 - 3) + \mathcal{M}(I_2 - 3) + \mathcal{A}(I_3 - 1)$$

where  $\mathcal{H}$ ,  $\mathcal{M}$ , and  $\mathcal{A}$  are at least functions of  $I_1$ ,  $I_2$ , and  $I_3$  and perhaps their derivatives. The most trivial case would be  $\mathcal{H} = C_1$  (const),  $\mathcal{M} = C_2$  (const), and  $\mathcal{A} = C_3$  (const).

Figs. 50, 51, and 52 show point strain energy vs. strain invariant relationships for resin sheet 283C, resin motor sheet ( $\epsilon_1/\epsilon_2 \approx 1$ ), and resin motor sheet ( $\epsilon_1/\epsilon_2 \approx 2$ ), respectively. The relationships are somewhat nonlinear for at least small strains. An excellent comparison between strain energy versus strain invariants can be had by comparing the uniaxial strain energy and the inflated cylinder strain energy in Table 8 of QSR-12 with that of Figs. 51 and 52. This correlation indicates that the proposed theory and experimental techniques definitely characterize rubber in the small strain realm.

Finally, for completeness, strain energy versus the invariants are shown for the dummy propellant in Fig. 53. The data scatter precludes any obvious curve fitting. However, if the dashed lines are assumed to be average representations of the data, then correlation is found with the data obtained from the inflated cylinder test (Fig. 17, QSR 38-10).

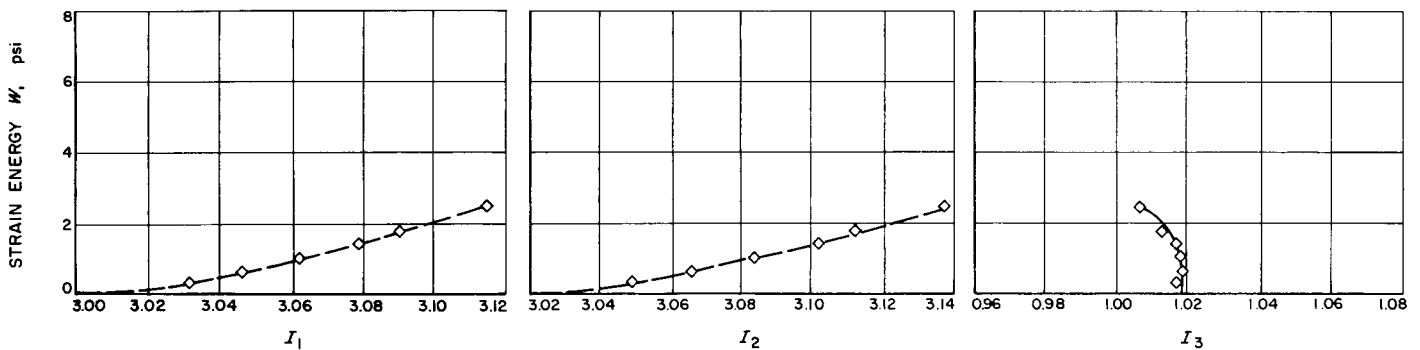


Fig. 50. Strain energy versus the three invariants (resin 283C "sheet"  $\epsilon_1/\epsilon_2 \approx 1$ )

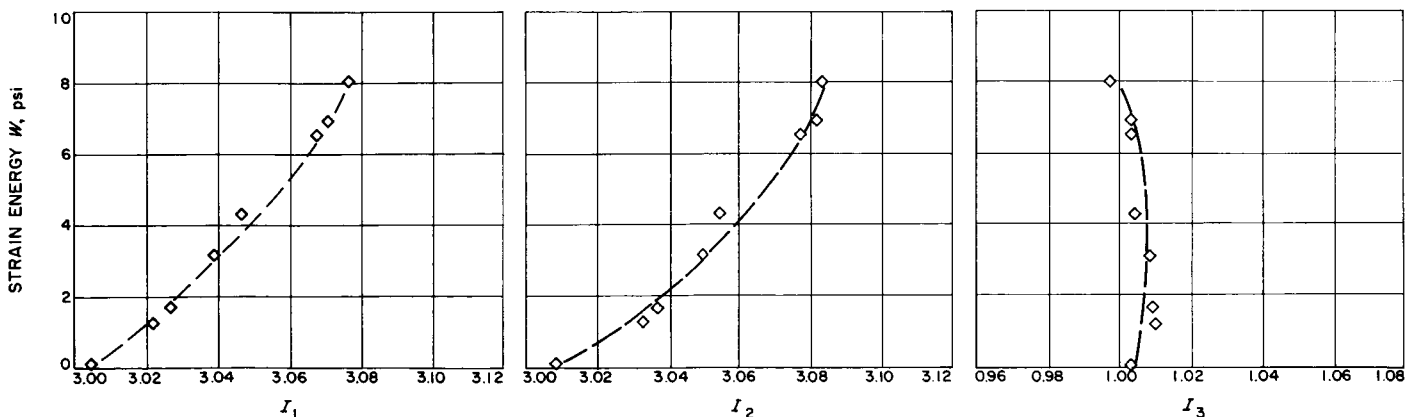


Fig. 51. Strain energy versus the three invariants (resin motor "sheet"  $\epsilon_1/\epsilon_2 \approx 1$ )

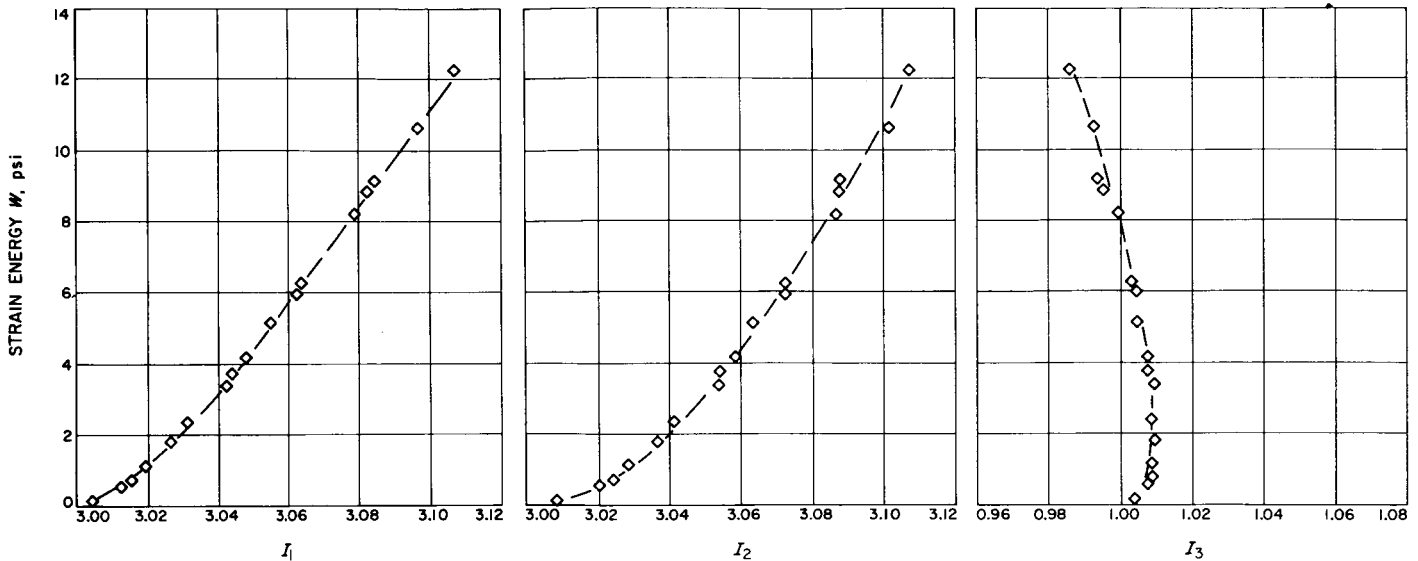


Fig. 52. Strain energy versus the three invariants (resin motor "sheet"  $\epsilon_1/\epsilon_2 \approx 2$ )

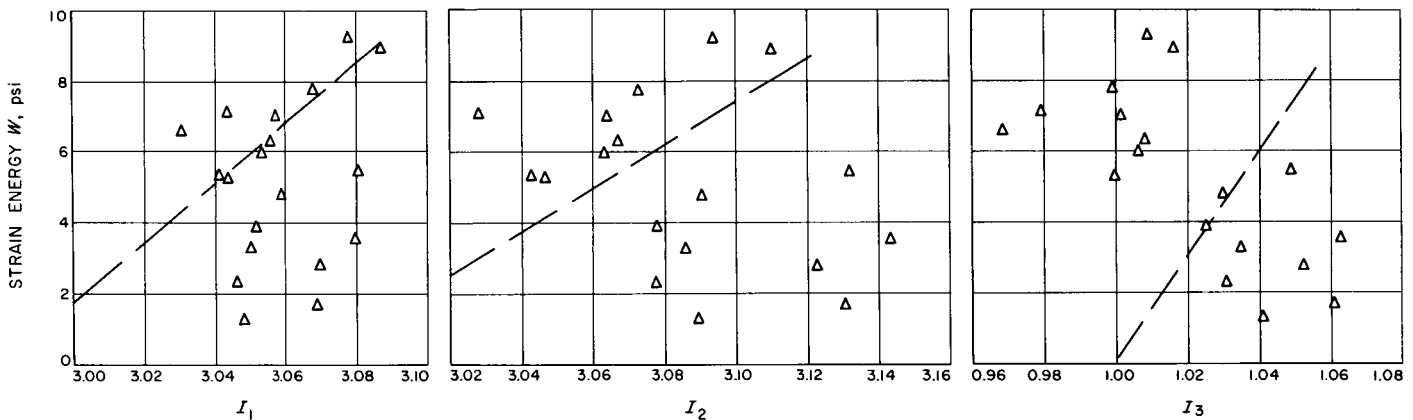


Fig. 53. Strain energy versus the three invariants (dummy propellant "sheet"  $\epsilon_1/\epsilon_2 \approx 2$ )

## 7. Conclusion

The first phase of construction of a tension-tension biaxial sheet tester has been completed. A method was presented to evaluate the approximate stress magnitudes at the center of a biaxially stressed propellant sheet. Rough data obtained from this instrument was compared with the proposed theory of this study program, together with results from the inflated cylinder test. A correction to a previous statement regarding the functional form of

$H$ ,  $W$ , and  $R$  was made, stating that they were functions of the invariants and possibly their derivatives, but *not* the leading partial derivatives of a Taylor expansion. This correction has in no way altered any of the reported data and observations of previous QSR's. It was shown that the theory and experimental techniques proposed in this study are at least applicable for unfilled polyurethane. Hence, one basis for the advanced study of non-linear viscoelasticity has been established.

## References

1. Rapp, N. S., and Ingham, J. D., "Polymer Degradation Mechanisms: C<sup>14</sup>-Labeled Polyoxypropylene Glycol-Toluene Diisocyanate Polymers," *Space Programs Summary* No. 37-23, Vol. IV, pp. 104-108, October 31, 1963; and *Quarterly Summary Report* No. 38-13, pp. 12-15, October 31, 1963 (Confidential).
2. Conway, D., and Libby, W. F., "The Measurement of Very Slow Reaction Rates; Decarboxylation of Alanine," *Journal of the American Chemical Society*, Vol. 80, pp. 1077-1084, 1958.
3. Rapp, N. S., and Ingham, J. D., "Polymer Degradation Mechanisms: Polyoxypropylene Ethers and Polyurethanes," *Space Programs Summary* No. 37-22, Vol. IV, pp. 108-118, August 31, 1963.
4. Landel, R. F., Moser, B. G., and Bauman, A. J., "Rheology of Concentrated Suspensions: Effect of a Surfactant," presented at the 4th International Congress of Rheology, Brown University, August 26, 1963 (to be published in the *Proceedings*).
5. Moser, B. G., Landel, R. F., and Bauman, A. J., "Rheology of Suspensions: Implications of Surfactants for High Energy Systems" (Confidential), presented at the Second Annual Meeting of the Working Group on Mechanical Behavior, Interagency Chemical Rocket Propulsion Group, at Hill Air Force Base, November 19, 1963 (to be published in the preprints).
6. Smith, T. L., "Failure Envelope for Characterizing Ultimate Tensile Properties of Amorphous Elastomers," Preprints, Division of Organic Coatings and Plastics Chemistry, Chicago Meeting of the American Chemical Society, September 1961.
7. Landel, R. F., and Fedors, R. F., "Rupture Behavior of Elastomers: Effect of Statistical Variability and Cross-Link Density," *Polymer Letters*, Vol. 1, p. 539, 1963.
8. Landel, R. F., and Fedors, R. F., "The Tensile Failure Envelope of Amorphous Elastomers: Effects of Statistical Variability and Cross-Link Density," *Transactions of the Society of Rheology*, Vol. 7 (in press).
9. Smith, T. L., "Ultimate Tensile Properties of Elastomers: Dependence of the Failure Envelope on Cross-Link Density," Paper presented at the 4th International Congress on Rheology, Brown University, Providence, R. I., 1963.
10. Lal, J., and McGrath, J. E., "Vulcanization of Poly (vinyl alkyl ethers) with Dicumyl Peroxide and Sulfur," *Rubber Chemistry and Technology*, Vol. 36, p. 1159, 1963.
11. Novikov, A. S., Galil-Ogly, F. A., and Gilinskaya, N. S., "Fluoro-Elastomer Vulcanizates of the 'Viton A' Type Containing Benzoyl Peroxide," *Soviet Rubber Technology*, No. 2, p. 5, 1962.
12. Novikov, A. S., Galil-Ogly, F. A., Gilinskaya, N. S., and Nudelman, E. N., "Vulcanization of Viton-type Fluoro-Elastomers with Hexamethylene Diamine," *Soviet Rubber Technology*, No. 3, p. 5, 1962.
13. Smith, T. L., "Mechanisms of Reversible and Irreversible Loss of Mechanical Properties of Elastomeric Vulcanizates Which Occur at Elevated Temperatures," ASD-TDR-62-572 Report, Wright-Patterson Air Force Base, Ohio, June 1962.

## References (Cont'd)

14. Smith, T. L., "Ultimate Tensile Properties of Elastomers. II. Comparison of Failure Envelopes for Unfilled Vulcanizates," *Journal of Applied Physics*, Vol. 35 (in press).
15. Martin, G. M., Roth, F. L., and Stiehler, R. D., "Behavior of 'Pure Gum' Rubber Vulcanizates in Tension," *Transactions of the Institute of Rubber Industries*, Vol. 32, p. 189, 1956.
16. Treloar, L. R. G., *Proceedings of the Physical Society*, London, Vol. 60, p. 135, 1948.
17. Rivlin, R. S., *Philosophical Transactions of the Royal Society*, Vol. 243, p. 251, 1951.
18. Blatz, P. J., and Ko, W. L., *Transactions of the Society of Rheology*, Vol. 6, p. 223, 1962.
19. Monch, E., and Galster, D., *British Journal of Applied Physics*, Vol. 14, p. 810, 1963.
20. Noll, W., and Truesdell, C., "The Non-Linear Field Theories of Mechanics," Vol. 3, Part 3, S. Flugge, Ed., Springer-Verlag, Berlin, 1964 (in press).